A Study of Simplified Models for Dark Matter Searches in pp Collisions

von
Harun Acaroğlu

Bachelorarbeit in Physik
vorgelegt der
Fakultät für Mathematik, Informatik und Naturwissenschaften
der RWTH Aachen
im Oktober 2015

angefertigt im
III. Physikalischen Institut A

bei
Herrn Prof. Dr. Thomas Hebbeker

Abstract

A study of different model approaches for missing $\not{E}_T$ searches in the mono-lepton channel with a lepton plus $\not{E}_T$ in the final state. In the first part of this analysis dark matter is considered to be a Majorana fermion. It is found, that compared to the usual Dirac fermion approach there is no difference regarding the kinematics but a difference of a factor of two on the cross section in the Majorana case.

A short analysis of non integer coupling values for the mediators coupling to quarks shows, that this provides no fundamental changes for the process's kinematics.

Further, the interference, which is described by a parameter ξ, is analyzed. In contrast to an EFT, where cases of unequal couplings to up and down type quarks have been restricted, one finds a rather different behavior of the simplified model, when it comes to gauge invariance and unitarity. It is found, that this difference of behavior opens the cases $\xi = -1, 0$ for a simplified model within a certain range of validity.

Contents

Chapter 1

Introduction

1.1 Dark Matter

Starting with the very first attempts on describing nature from a rather philosophical point of view as it was done in the ancient Greece, physics has made a huge development. This development does not only consist of an enhancement and clarification of the insights; it also contains changes regarding the epistemology behind this science.
Modern physics like we know it from our days has its roots in the early 20th century. In this era *theoretical physics* was increasing in popularity, yielding a generation of very successful physicists - physicists like Einstein, Dirac or Heisenberg, who are known as founders of modern physics. The result of this persistent development is the empiric science we know from our days. Based on a symbiotic relation between the theory and experiment, physics of our time work in way where falsifiable theories make predictions, which have to be proven by the experiment. The most famous example for a successful application of this interplay of theory and experiment is the discovery of the *Higgs boson*. This particle was predicted by the theoretical physicists Peter Higgs, Robert Brout and Francois Englert in 1964 and was detected about 50 years later at the LHC experiment in 2012.
But this is not the only way how physics is performed nowadays. The four fundamental interactions we know today, namely the gravitational, electromagnetic, weak nuclear and the strong nuclear interactions, are described correctly by the standard model (SM) and the general theory of relativity (GTR), where the last mentioned describes gravitation. Besides problems within these working theories, like the lack of an explanation for the existence of three particle generations (SM) or the problems regarding a quantum theorie of gravitation (GTR), there are also some observations, which can not be explained by using these theories. Here, physicists are encouraged to work out new theoretical predictions and to perform new or adjust existing experiments for an appropriate analysis of this *new physics*.
One of these observations was a measurement of the rotational velocity of stars with regard to their distance from the center of galaxy (see fig.1.1). Besides assuming a varying gravitational constant in order to explain this result, one can introduce a new type of matter, called *dark matter* (DM). This sort of new matter is going to be the main subject of this bachelor thesis.

1.2 Dark Matter Candidates and Searches for Dark Matter

Although physicists have some hard evidence for the existence of dark matter, there is no real general consent regarding the nature of this new type of matter. Caused by this divergency of opinions there are a lot of possible candidates today [17]. The most general distinction one

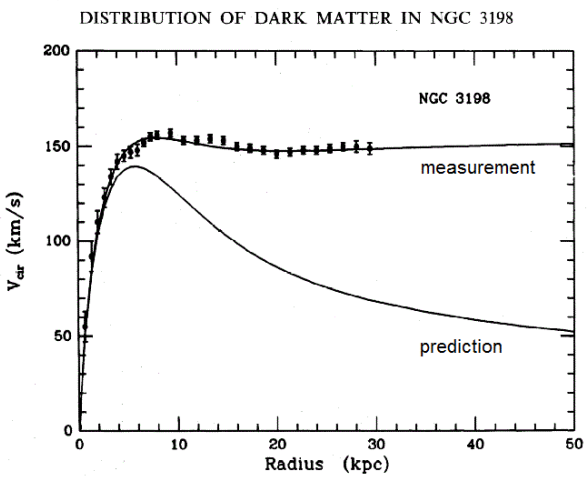

Figure 1.1: Example for such a measurement for the galaxy NGC 3198 (adapted from [33])

can make about this candidates is whether they are considered as baryonic or non-baryonic particles. Baryonic dark matter is rather considered in cosmological approaches. Most famous candidates of this sort are massive astrophysical compact halo objects (MACHOs). Non-baryonic candidates are considered to be new particles which do not couple to the photon and thus have no electrical charge. The most common framework in this category is the so called WIMP - a weakly interacting massive particle. This attempt supposes a particle, which is only involved in gravitational and weak interaction and is often complemented by the assumption to be a *Dirac* or *Majorana* fermion [17].
Besides different approaches regarding the candidates for DM there are also different ways of detecting or rather searching for the respective non-baryonic candidates. In general there are three ways of searching for dark matter (see also fig.1.2):

a) Direct detection:
In direct detection experiments physicists measure an energy emission, like for example the emission of a phonon in a solid, which is caused by the recoil of dark matter from standard model matter. Examples for such a search are the experiments LUX and XENON100 [17].

b) Indirect detection:
Experiments which try to measure the production of standard model matter caused by the annihilation of a DM pair are called indirect detection experiments. Here we can mention Ams and IceCube as known experiments [17].

c) Production at colliders:
Another way to search is to produce a DM pair at collider experiments like for example at the LHC's CMS experiment. Here one should be able to see a signal in the so called *transverse momentum spectrum* p_T. Since this is the kind of DM searches, which this thesis is concerning with, there will be a more detailed explanation of this in the following section [17].

In this thesis a simplified model, which has a WIMP approach implementation, will be used. This model describes the production of DM (labled as χ) with two quarks in the inital state and a lepton plus missing transverse energy ($\not{E}_T$) in the final state. The DM pair is produced by the decay of a new vector boson (labled as V_{med}) and the lepton plus a neutrino are produced by a decaying W boson (see fig.1.3). In this model DM is either assumed to

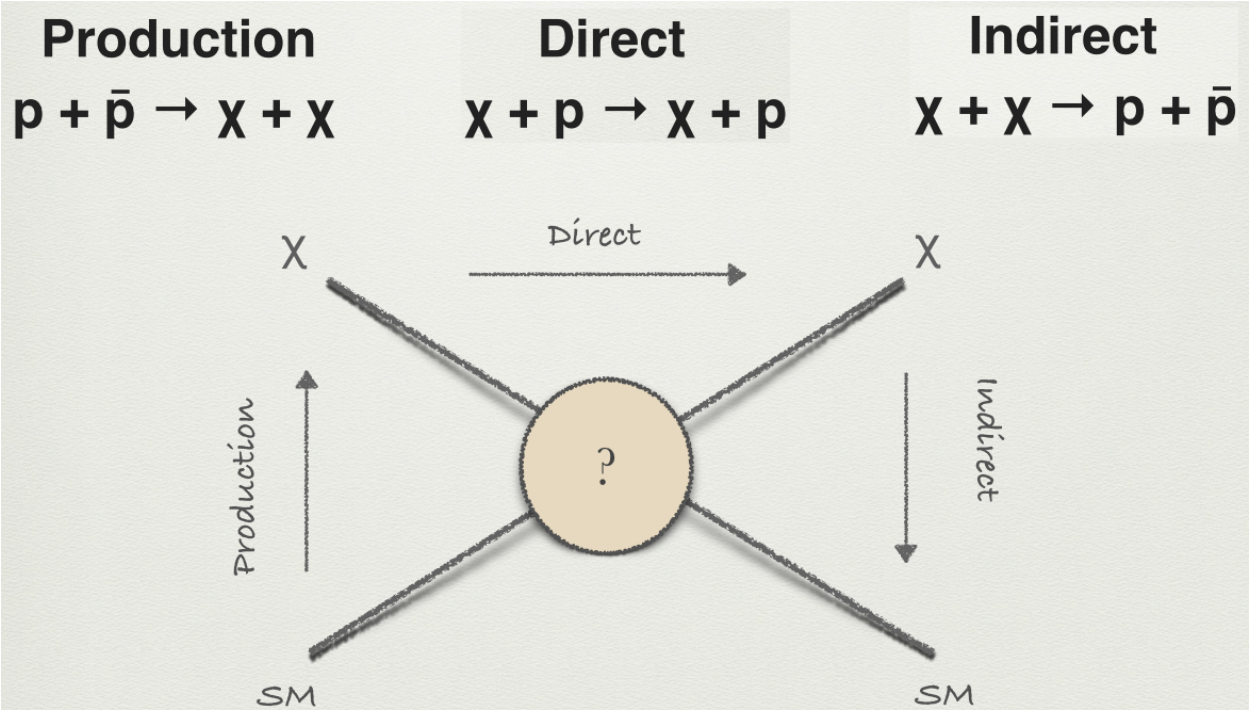

Figure 1.2: Three ways of searching (adapted from [30])

be a Majorana or a Dirac fermion. This thesis does a study on generator level for both approaches. The theoretical differences between the two spinors are also pointed out and discussed.
In both models unequal coupling of the new mediator to either up or down type quarks is considered as an interference. A parameter, which describes this interference, will also be introduced and there will be a discussion of its validity.

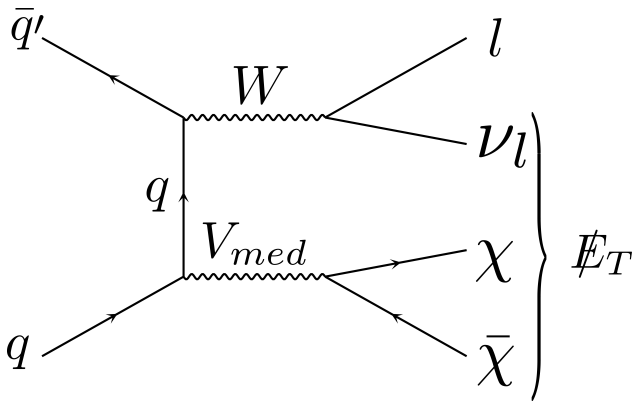

Figure 1.3: Feynman diagram for the mono-lepton channel

Chapter 2

Theoretical Framework

2.1 The Standard Model

Like mentioned in the introduction, the standard model of particle physics is able to explain and describe three out of four known fundamental physical interactions; the electromagnetic, weak and strong interaction. This theory was acquired in the second half of the 20th century and can make precise predictions even when it comes to interactions on a subatomic scale and thus is considered as one of the most successful theories. Although many of its predictions have been proven by experiments, there are still aspects, where a description within the standard model or finding an explanation based on it fails. The existence of three fermion generations was already mentioned as one of these aspects. Another example is the lack of an explanation for the difference in the energy scale of weak and gravitational interaction.
The standard model of particle physics is a quantum field theory. This means, that its fundamental objects are quantized fields appending to respective particles. Since it is symmetric under several gauge transformations, the standard model is also a gauge theory. It satisfies the laws of special relativity, what makes it a *relativistic quantum field theory*.
The particles of the standard model can be divided in two categories, namely *fermions* and *bosons*. Fermions are particles with half-integer spin. Within fermions the theory makes a distinction regarding leptons - like the electron and its neutrino - and quarks - like the up and down quark. Furthermore there are three generations of fermions, which are only differing in their mass. Matter is composed of this kind of particles.
Particles with an integer spin are called bosons. In the standard model these are those particles, which mediate the known forces. For each known force there exists a respective boson. The strong force is mediated by the gluon and is only participated by quarks. This kind of interaction is described by a type of charge - the so called color. The electromagnetic force is mediated by the photon, which couples to electrical charged leptons or quarks. Z bosons as well as $W^{\pm}$ bosons are mediating the weak force, which is participated by every fermion. Besides these five bosons there is also the Higgs boson. This particle is the excitation of a so called *higgs field*, which gives the SM particles their rest mass. Fig. 2.1 shows a table of the described particles [22, 23].

2.2 Detecting Dark Matter with the CMS

Some brief information on the *Large Hadron Collider's* (LHC) *Compact Muon Solenoid* (CMS) detector will be given in this section, as this thesis is related to a possible detection of DM at this detector. Furthermore, important quantities that are used in the analysis will

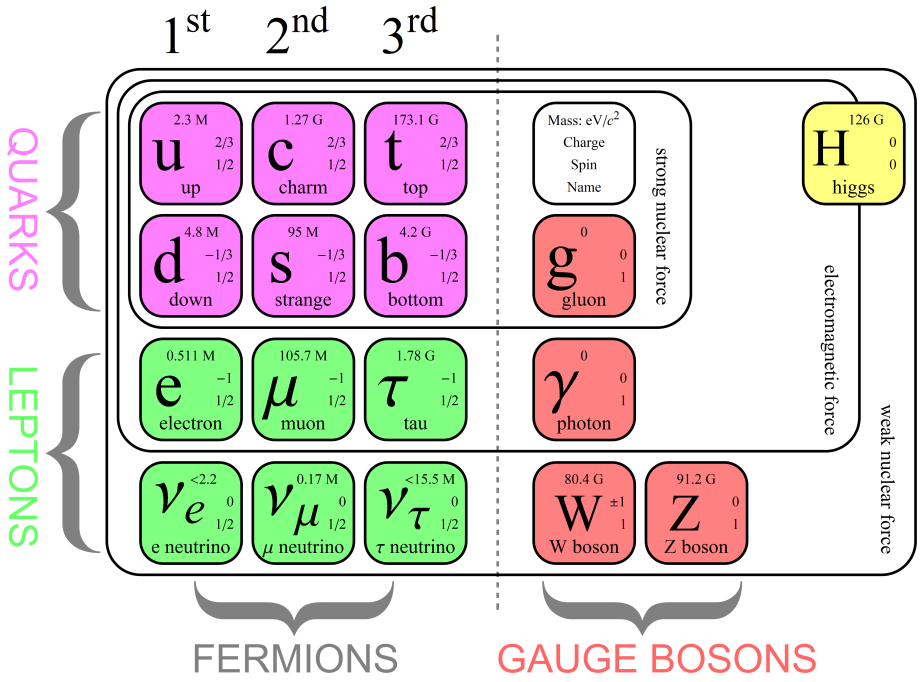

Figure 2.1: A compact table describing the particles of the standard model [34]

be introduced and in some cases theoretically derived.
The CMS detector was build within the scope of the LHC experiment [31]. Beside ATLAS it is rated as one of the two biggest detectors of the LHC and was build as a general-purpose detector [31]. Therefore it is used for several searches, including the search for the Higgs boson and searches for evidence regarding *Supersymmetry* (SUSY) [17,25,31]. The technical structure of this detector is reflecting its purpose of use. In order to be able to measure several particles, it has a layer structure, where every part of this layer is relevant for the measurement of a respective type of particle. From the core to the outside the layer structure is as follows [31] :

- **Silicon Trackers:**
  This tracker is supposed to register and measure the particle momenta by recording the particles' path. It is entirely made of silicon what provides a reasonable radiation hardness, since this can be a problem at the center of the detector, due to the high particle density. The inner part is constructed of pixel sensors, due to their high granularity and the outer part is constructed from silicon strip sensors.

- **Electromagnetic Calorimeter (ECAL):**
  The function of this layer is to measure the energy of particles forming an electromagnetic shower, such as photons and electrons. It is comprised out of a lead tungstate ($PbWO_4$). The electromagnetic shower is connected to the energy of the particles.

- **Hadronic Calorimeter (HCAL):**
  With this sampling calorimeter hadronic particles like neutrons and protons are measured. It is made out of bass, which is due to the density of this material. Furthermore it has a plastic scintillator coating in form of tiles.

- **The magnet:**
  The CMS has a solenoid magnet, which can produce a field strength of up to 3,8 T. It is placed in the very center of the detector to provide this magnet field for the other

layers. The magnet field is of particular importance, since it bends electrically charged particles depending on their momenta.

- **Muon chambers:**
  Muons have a mass 200 times larger than electrons. They pass the calorimeters and the magnet and one therefore needs another detector in order to measure them. In the CMS this is solved by gaseous chambers. In the barrel region the trajectory of the muons is measured by *drift tubes* and in the end cap by so called *cathode strip chambers*. Within both regions there are *resistive plate chambers*, which are used as a muon trigger.

A more detailed presentation of the layer structure of the CMS experiment can be seen in fig. 2.2, while fig. 2.3 shows the typical trajectory for several particles in the CMS.
A very important kinematic quantity for measurements with the CMS is the so called *transverse mass* M_T. A short derivation of this quantity for the example of a W^+ boson decaying into a μ^+ and a ν_μ (see fig. 2.4) will be done. In this derivation the beam direction is the z-axis and natural units will be used.

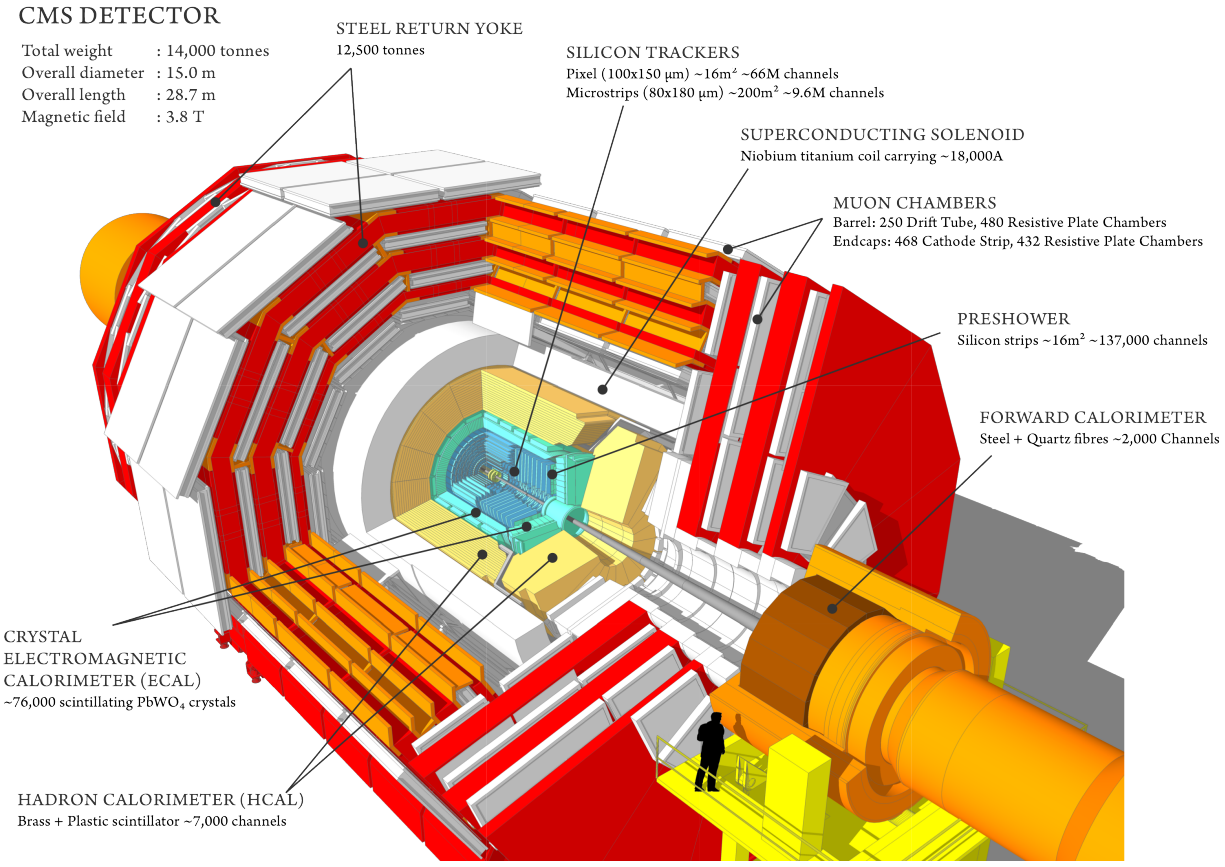

Figure 2.2: Layer structure of the CMS [31]

Let us start with the invariant mass of the W boson which is defined as

$$m_W{}^2 = E_W{}^2 - \vec{p_W}{}^2. \tag{2.2.1}$$

By using momentum conservation one can derive that

$$\begin{aligned} {m_W}^2 &= (E_\mu + E_\nu)^2 - (\vec{p}_{\mu,T} + \vec{p}_{\nu,T})^2 - (p_{\mu,z} + p_{\nu,z})^2 \quad , \\ \text{with} \quad \vec{p} &= \begin{pmatrix} p_x \\ p_y \\ p_z \end{pmatrix} = \begin{pmatrix} \vec{p}_T \\ p_z \end{pmatrix} \quad , \end{aligned} \tag{2.2.2}$$

where the momentum along the beam axis of the neutrino (denoted by "$p_{\nu,z}$") is unknown, since it is not measured by the detector. However, the transverse momentum (denoted by "$p_{\nu,T}$") can be calculated back by using that the total transverse momentum has to be conserved, too. For the missing transverse momentum $\vec{\not{p}}_T$ one then gets

$$\vec{\not{p}}_T = -\Sigma \vec{p}_T^{\,observed} \quad , \tag{2.2.3}$$

whereby this quantity can be identified as $\vec{p}_{\nu,T}$ in this case.

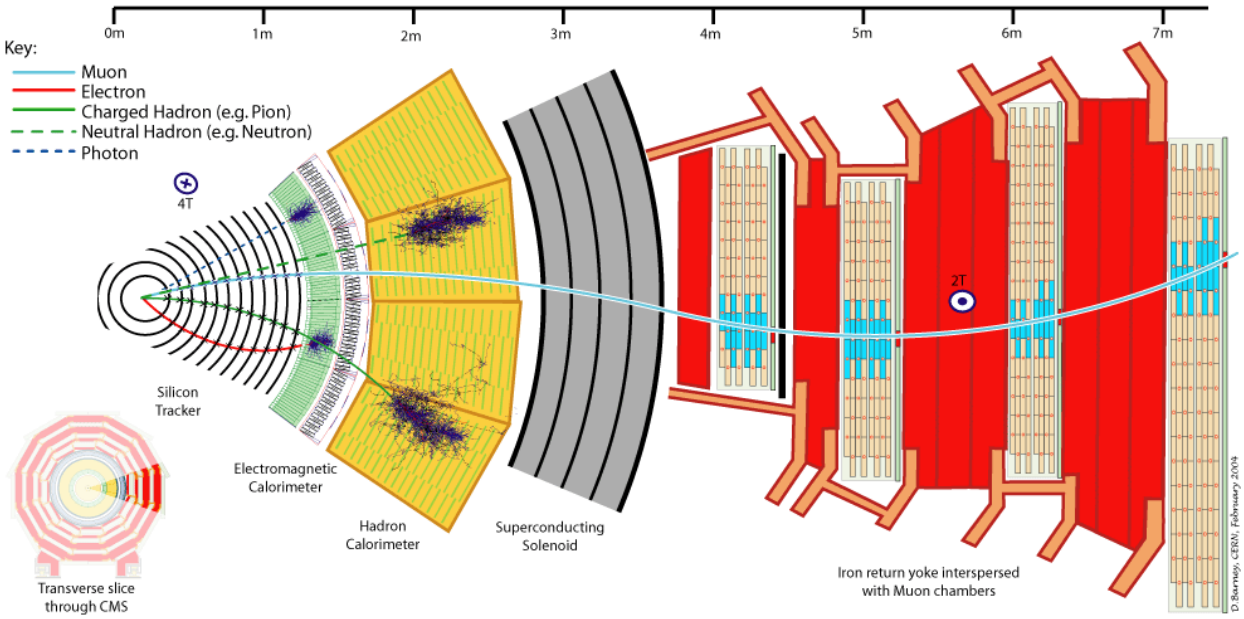

Figure 2.3: Transverse slice of the CMS detector and typical particle trajectories [32]

One can now ignore the longitudinal motion of the lepton system, since the neutrino's longitudinal momentum is unknown, and rather use only transverse variables. The transverse mass is then defined as

$${M_T}^2 = (E_{\mu,T} + \not{E}_T)^2 - (\vec{p}_{\mu,T} + \vec{\not{p}}_T)^2 \quad , \tag{2.2.4}$$

with $E_T^2 = m^2 + \vec{p}_T^{\,2}$ as the transverse energy of each particle. By plugging this relation into the transverse mass one finally finds that

$$\begin{aligned} {M_T}^2 &= (E_{\mu,T} + \not{E}_T)^2 - (\vec{p}_{\mu,T} + \vec{\not{p}}_T)^2 \\ &= E_{\mu,T}^2 + {\not{E}_T}^2 + 2 \cdot \not{E}_T \cdot E_{\mu,T} \\ &- |p_{\mu,T}|^2 - |\not{p}_T|^2 - 2 \cdot \vec{p}_{\mu,T} \cdot \vec{\not{p}}_T \\ &= m_\mu^2 + m_\nu^2 + 2 \cdot (\not{E}_T \cdot E_{\mu,T} - \vec{p}_{\mu,T} \cdot \vec{\not{p}}_T) \quad . \end{aligned} \tag{2.2.5}$$

The mass of the W boson puts a cap on this quantity. If the lepton and neutrino are produced with an angle of 180° in between them (back to back), then there is no longitudinal momentum at all ($\vec{p}_{\mu,z} = -\vec{p}_{\nu,z}$). For this case we get that $M_T = m_W$ and generally one finds that $M_T \leq m_W$.
For the case of a much greater mass of the mother particle (the W boson in our frame) than the daughter masses ($m_W^2 - m_\mu^2 - m_\nu^2 \approx m_W^2$) one can make the approximation that $m_\mu = m_\nu = 0$ and the expression for E_T simplifies to $E_T = |\vec{p}_T|$. Using this leads to

$$M_T = \sqrt{2 \cdot |\vec{p}_{\mu,T}| \cdot |\vec{\not{p}}_T|(1 - \cos\phi)} \quad , \tag{2.2.6}$$

where ϕ is the angle between $\vec{p}_{\mu,T}$ and $\vec{\not{p}}_T$ [19, 20].
For a general decay, where particle 1 decays into a visible particle 2 and a non-visible particle 3 we get that

$$M_T = \sqrt{2 \cdot |\vec{p}_T| \cdot |\vec{\not{p}}_T|(1 - \cos\phi)} \quad , \tag{2.2.7}$$

with ϕ being the angle between the visible and non-visible particle [19, 20].

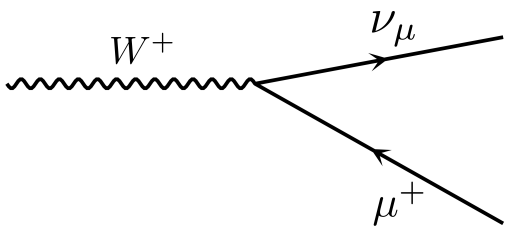

Figure 2.4: Feynman diagram for a W^+ decay

Beside the transverse mass there are two other quantities which will be used in this analysis. One of them is the azimutal angle of the transverse plane through the detector. Since the detector is build cylindrical one can put the z-axis onto the beam and use cylindrical coordinates. The angle ϕ would then equal the angle ϕ one knows from cylindrical coordinates. The physics in the LHC can be considered ϕ-invariant, since there is a general cylindrical symmetry. For single events the ϕ distribution is very important.
Another important geometric quantity is the so called *pseudorapidity* η. This quantity is defined as

$$\eta = -ln\left[tan\left(\frac{\theta}{2}\right)\right] \quad , \tag{2.2.8}$$

with θ being the usual polar angle one knows from spherical coordinates. It can be measured through the momentum of the detected particles since it also follows the equation

$$\eta = \frac{1}{2} ln\left(\frac{|\vec{p}| + p_L}{|\vec{p}| - p_L}\right) \quad . \tag{2.2.9}$$

With this two quantities one can access the geometry of the events and read out the polar as well as the azimutal distribution of them.
Since this distributions and the transverse mass are fundamental quantities reflecting the kinematics behind the treated process they will be used to quantifiy possible differences between the analyzed models.

2.3 Simplified Models for Dark Matter

2.3.1 Simplified Models in General

Simplified Models are less incomplete models than *effective field theories* (EFTs), since they have a mediator implementation (see fig.2.5) [1–6]. EFTs on the other hand are models, where non-renormalizable operators describe the process of interest. For the case of searches for DM in missing energy signatures one has such operators coupling the standard model partons to a field that represents the DM WIMP's. An example for such an operator would be

$$\mathcal{L}_{EFT} = \frac{1}{\Lambda^2}(\bar{q}q)(\bar{\chi}\chi) \quad , \tag{2.3.1}$$

with Λ being the interaction scale of the process [1]. Operators like this can describe many important processes like the scattering of a WIMP on quarks or an annihilation process, where a pair of WIMP produces two quarks. They can also describe our process of interest, namely the production of a WIMP pair through the annihilation of a pair of quarks. An analysis of such an EFT model for mono-lepton searches was done in [8, 15].

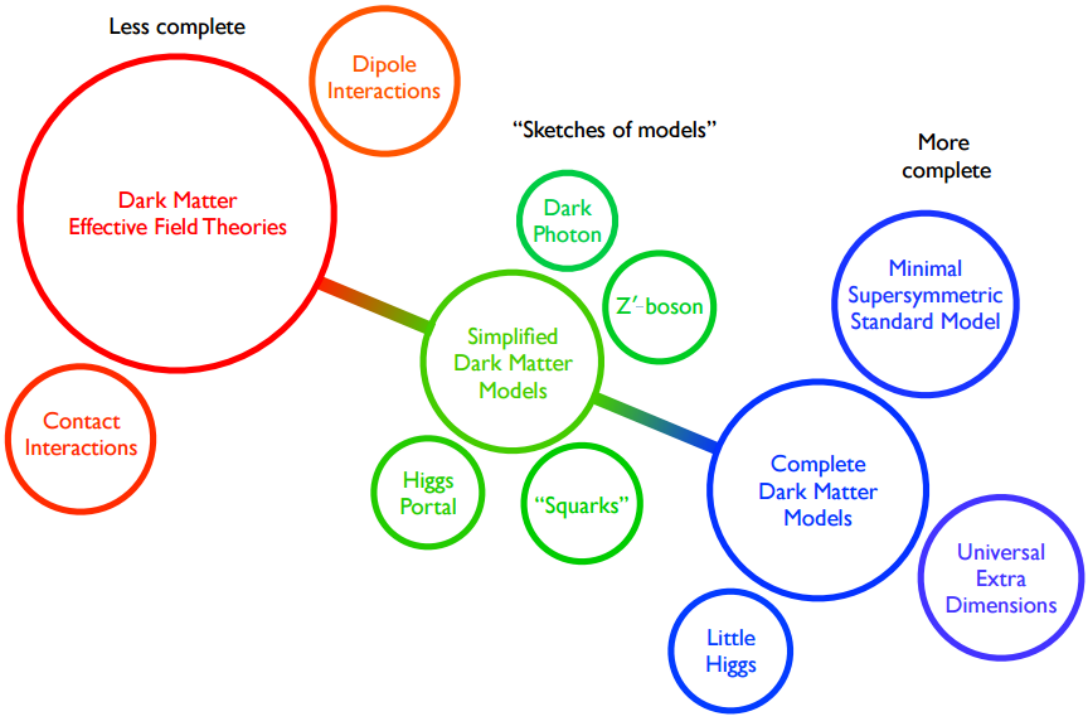

Figure 2.5: Illustration of different model approaches [4]

In an EFT one considers interactions of a model with a mediator at an energy scale much smaller then the mass of this mediator M_{med}. For such interactions one can ignore the intermediate state and contract two vertices into one. Then perturbation theory can be applied in order to calculate the physical processes, since their energy can be developed in a power series like E^n/Λ^n [1]. Just this is the main point where simplified models start to be anticipated. This approach is only consistent, if one describes processes with an energy smaller than the interaction scale Λ. To justify the usage of simplified models it will be demonstrated how strict the constraints on an EFT are, if it is applied to an s-channel process like shown in figure 2.6.

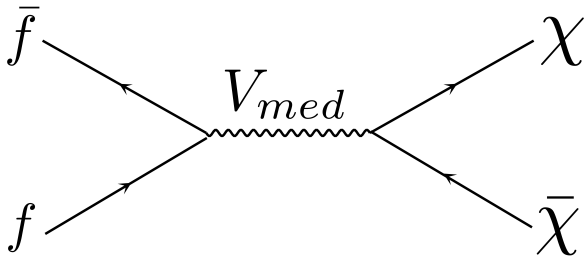

Figure 2.6: Annihilation of fermions producing a DM pair

The EFT approach is valid for energies, for which the mediator can not be produced produced and one can therefore neglect the respective intermediate state and contract two vertices [1,6]. Mathematically this gives us the following equation:

$$Q < M_{med}. \tag{2.3.2}$$

For a simple calculation one can make the assumption that the partons within a proton carry always a third of the proton systems center of mass energy $\sqrt{s}$. Although a proper description needs *parton distribution functions* (pdfs) to be considered, here they will be neglected for the course of simplicity. Within this framework one would expect the transferred momentum to be

$$Q = \frac{\sqrt{s}}{3}. \tag{2.3.3}$$

For s-channel kinematics one additionally finds the relation [1], that

$$Q > 2m_{\chi}. \tag{2.3.4}$$

One can now use equations 2.3.2-2.3.4 to derive bounds on the mediator and DM masses:

$$2m_{\chi} < \frac{\sqrt{s}}{3} < M_{med}. \tag{2.3.5}$$

The center-of-mass energy $\sqrt{s}$ of the LHC's current run and therefore also of this analysis' simulations is 13 TeV. At such high energies it is earnestly questionable, if the EFT should still be used for analyses, since this makes very strong restrictions on the mediator mass:

$$2m_{\chi} < 4333 \text{ GeV} < M_{med}. \tag{2.3.6}$$

Considering the upper mentioned pdfs does even strengthen this lower bound of the mediator mass, since the pdfs give several partons a probability to carry even a greater fraction of the center of mass energy. At this point the simplified model proofs itself as a more appropriate framework, since one does not need to worry about such bounds [1–6]. The fact that it has implemented a mediator particle solves this particular problem and opens possibilities for further analyses. Nevertheless, one has to be careful with simplified models as well. If one considers sufficiently small mediator masses, the mediator can be produced on-shell. In such a case it would be necessary to also consider processes other than the production of a dark matter pair, since the mediator could and necessarily will decay into quarks [1]. The interesting point here is each branching ratio, with which the mediator decays either into dark matter or into quarks. Since this branching ratio would just scale the cross section for the mono lepton channel [26] and this analysis consists out of a shape analysis only, this can be neglected. Summarized one has to register, that with respect to an EFT more general assumptions have to be made for a simplified model, since it has a mediator implementation.

2.3.2 The Models Used in this Analysis

The models that will be used in this analysis can be considered as one model with two versions: one with a Dirac spinor implementation and one where the DM particle is described by a Majorana spinor. Due to this they will be referred to in the following as just one model. This simplified model has a vector mediator which does only couple to dark matter and quarks through an axial vector interaction. An axial vector is defined as follows [16]

$$A^{\mu}(x) = \bar{\psi}(x)\gamma^{\mu}\gamma_{5}\psi(x) \quad . \tag{2.3.7}$$

Its most important properties are its antisymmetric behavior under parity transformations and charge conjugation ($A^{\mu}(x) \rightarrow A'^{\mu}(x') = -A_{\mu}$) [16]. The latter one will play an important role in the analysis of the Majorana model. Interactions which are described by an axial vector are always spin dependent [1, 5, 6, 16].
The choice to just use an axial vector coupling is not arbitrary. This was decided based on the results of [15]. Here it was found, that there is no significant difference between a vector coupling or an axial vector coupling. For reasons of limiting and a better significance it was decided to use only the axial vector coupling models.
Like mentioned above, the mediator of this model is a vector boson. This means that it is a spin 1 particle. It furthermore is a color singulet and therefore has no color. The Lagrangian term for the dark matter process of such a model is

$$\mathcal{L} \supset \frac{1}{2}M_{med}^{2}V^{\mu}V_{\mu} - g_{\chi}V_{\mu}\bar{\chi}\gamma^{\mu}\gamma_{5}\chi - \sum_{u=q,d} g_{q}V_{\mu}\bar{q}\gamma^{\mu}\gamma_{5}q \quad , \tag{2.3.8}$$

where u and d stands for either up or down type quarks [1, 5, 6] . The sum over q plays an important role for the interference parameter ξ, which will be explained further in the next paragraph.
Other quantities in this operator are V^{μ}, which describes the mediator, and g_{χ}, the coupling constant for how it couples to DM. In this analysis it will not be used as a parameter and set to a constant value through all simulations[1]. The mediator is assumed to decay only into a pair of DM.[2]
Further parameters of this model are the mediator mass M_{med}, the DM mass m_{χ} and the decay width of the mediator Γ_{med}. The DM particle is assumed not to decay into other products. For the width of the mediator Γ_{med} the so called narrow width approach will be followed, with

$$\Gamma_{med} = \frac{M_{med}}{8\pi}. \tag{2.3.9}$$

In this approach the mediator is assumed to couple only to one quark and color [27]. This choice is justified, since this analysis investigates the shape of M_T spectra and it was found in an earlier work [26], that changes in the width of the mediator do not cause changes in the shape, but scale the spectrum. Finally this reduces the number of parameters for this analysis to three: the masses M_{med} and m_{χ} as well as the coupling parameter ξ.

2.3.3 The Parameter ξ

It was mentioned above that there is a sum over the mediator either coupling to up or down type quarks in the Lagrangian. With choices of an unequal (equal) sign for the mediator's coupling to up and down type quarks one can produce cases of constructive (destructive) interference (see fig.2.7) [8, 15]. This interference is parameterized by ξ, which is defined as

[1] This parameter is set to $g_{\chi} = 1$.
[2] Even for masses small enough to produce the mediator on-shell this assumption will be maintained.

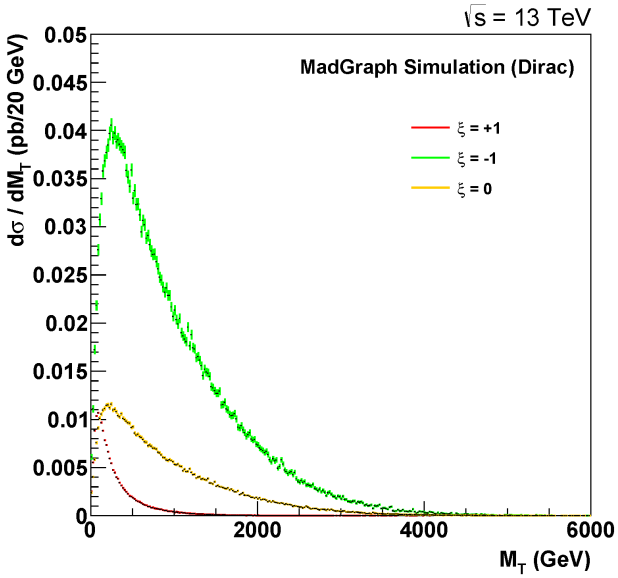

Figure 2.7: Illustration of the the interference cases. $M_{med} = 1600$ GeV, $m_\chi = 10$ GeV.

follows.
Running the sum in the Lagrangian (see eq.2.3.8) gives

$$\sum_{q=u,d} g_q V_\mu \bar{q}\gamma^\mu\gamma_5 q = g_u V_\mu \bar{u}\gamma^\mu\gamma_5 u + g_d V_\mu \bar{d}\gamma^\mu\gamma_5 d. \tag{2.3.10}$$

Factorizing this expression yields

$$\begin{aligned} & g_u V_\mu \bar{u}\gamma^\mu\gamma_5 u + g_d V_\mu \bar{d}\gamma^\mu\gamma_5 d \\ =& g_u \left(V_\mu \bar{u}\gamma^\mu\gamma_5 u + \underbrace{\frac{g_d}{g_u}}_{\xi} V_\mu \bar{d}\gamma^\mu\gamma_5 d \right). \end{aligned} \tag{2.3.11}$$

In [15] it was found that

$$\sigma|_{g_u=0} \approx \sigma|_{g_d=0}, \tag{2.3.12}$$

and since same final states are produced one also finds that

$$\sigma \propto |g_u \mathcal{M}_u + g_d \mathcal{M}_d|^2, \tag{2.3.13}$$

where $\mathcal{M}_{u,d}$ is the matrix element for the respective coupling. For $g_{u,d} \in$ {-1,0,1} one can use the upper relations and define ξ to be the coupling to down quarks g_d only and set $g_u = 1$ (see fig.2.8). With this definition one can produce every case of interference, since it does not matter for the cross section which coupling constant has a negative sign, due to relation 2.3.13. The only case that can not be produced with this definition is the case $g_u = 0$, which is also not a problem in connection with equation 2.3.12. One therefore has a properly defined parameter describing the interference in this channel.
Nevertheless, this definition has to be treated with caution. It is just appropriate as long as one investigates $g_{u,d} \in$ {-1,0,1}. For analyses with non-integer couplings or couplings with $|g_{u,d}| > 1$ it is necessary and much more beneficial to just refer to the couplings as two

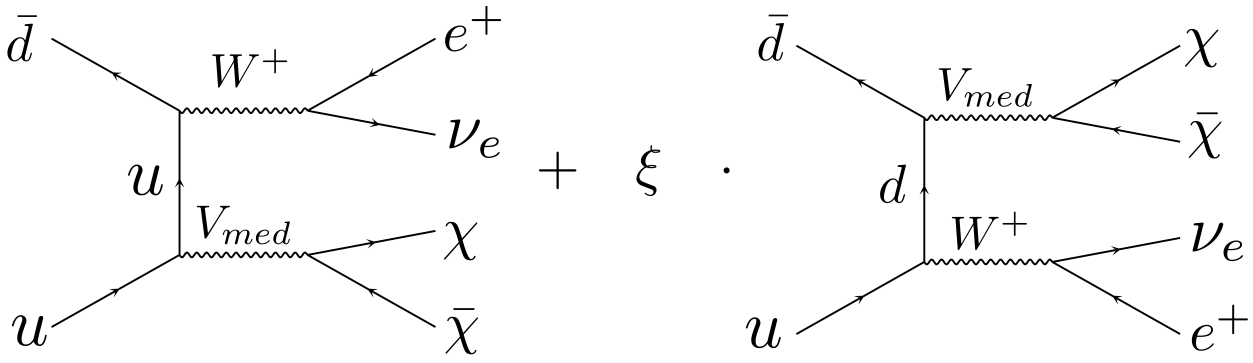

Figure 2.8: Illustration of the parameter ξ's definition

parameters, instead of defining something new.
A further analysis of this parameter will be an important part of this thesis. For an EFT there is a paper in which it is shown, that the cases $\xi = -1, 0$ cause problems regarding gauge invariance [7]. For the sake of a better understanding of this analysis and a better overview it was decided to split the theory section. Further theoretical insights will thus be given as an introduction to each part of this work. Especially when it comes to the validity of ξ there will be a larger theoretical introduction, where the above mentioned paper will be discussed further. Majorana spinors will also be introduced with the discussion of some theoretical aspects at the respective section.
In this analysis non-integer values for ξ will also be considered, where the definition from above will not be maintained.

Chapter 3

Computational Setup and Analysis

3.1 Event Generation

The events of this analysis are generated by the Monte Carlo event generator MadGraph 5 v2.2.3. The author of the MadGraph model is Mathieu Pellen, a theoretical physicist from the RWTH's Institute for Theoretical Particle Physics and Cosmology. The center of mass energy of the simulations is $\sqrt{s} = 13$ TeV. The simulation is performed up to leading order with one jet at matrix element level.
The simulated process is shown in figure 1.3. The number of events that were generated for each analysis is 200000. The cut on p_T is at 20 GeV and jet matching is put to MLM.
For different purposes of this analysis the parameters of the model are changed to various values. In the investigations on Majorana DM the mediator mass M_{med} is varied between 70 GeV and 3000 GeV and the DM mass m_χ is varied between 10 GeV and 2499 GeV. In order to investigate the interference, ξ is also varied between {-1,0,1}. For the analysis of a coupling structure between the mediator and DM, which shall resemble the standard model's photon's coupling[1], the coupling constants g_u and g_d are put to the values $\pm\frac{2}{3}$ and $\mp\frac{1}{3}$.
For the discussion of the interference parameter's validity it was necessary to also perform three runs with an EFT model, where the paramter ξ is varied between {-1,0,1}. A further analysis required also several runs with both, the EFT as well as the simplified model, in different gauges, set by using the command "*set gauge unitary/Feynman*".

3.2 Analysis of the Output

The output of the event simulation is analyzed by the *lheanalyzer* from the *libs3a* library of RWTH Aachen's institute IIIa.
In order to compare the kinematics of the Dirac and Majorana model the M_T spectrum for each run and the angular distributions (ϕ, θ) for sum runs are plotted. The M_T spectra are also plotted normalized for the sake of a shape comparison. The same plots are made for non-integer coupling values.
The analysis of the polarization and validity of ξ required some more effort. In order to get the angle between the W boson and the lepton or neutrino one needs to perform a Lorentz boost into the W system. By using this, angle plots which quantify the polarization of the W boson were made. In the last section graphs, which show the parton level cross section versus the parton system's center of mass energy will also be shown.

[1] This will be further motivated later.

Chapter 4

Results and Discussion

4.1 Majorana Dark Matter

4.1.1 Theoretical Basics

A Majorana fermion is defined through a symmetric behavior under charge parity transformations[1] [9–13, 16]. For the particle this means, that it is its own antiparticle. Mathematically this can be expressed by

$$\chi = \chi^c \quad , \tag{4.1.1}$$

where χ is a solution of the Dirac equation and χ^c is defined as

$$\chi^c = C\bar{\chi}^T, \tag{4.1.2}$$

with $C = i\gamma^2\gamma^0$ and $\bar{\chi} = \chi^\dagger\gamma^0$. By using the definition of a Majorana particle (4.1.1) one can derive an important insight for such particles. Since vector quantities switch their sign under charge conjugation, one finds

$$\chi^c\gamma^\mu\chi^c = \bar{\chi}\gamma^\mu\chi = -\bar{\chi}\gamma^\mu\chi. \tag{4.1.3}$$

A consequence of the relation above is that Majorana particles do not have vector couplings [9], which correspondents to spin independent interactions.
A candidate for a Majorana particle is the neutrino. Neutrino masses can be explained by assuming the neutrino to be a Majorana particle [28]. In SUSY the neutralino, a very good candidate for dark matter, is also a Majorana particle [17, 25].

4.1.2 Results

In this sections the results of the Majorana model's analysis will be presented and discussed. The main strategy is to make a comparison to the Dirac model and point out differences as well as similarities.
In particular the parameters m_χ and M_{med} will be varied for all three cases of ξ. If one mass parameter is varied, the other one will be fixed. This variation aims to point out possibly different sensibilities of the two approaches towards one of these parameters.
For the investigation of the models' sensitivity towards M_{med} this quantity was scanned through $M_{med} \in \{70\text{ GeV}, 400\text{ GeV}, 1600\text{ GeV}, 2050\text{ GeV}, 3000\text{ GeV}\}$ and m_χ was fixed to 10 GeV. These are just arbitrary values, since this is a shape analysis with the goal to reveal disparities or similarities between the two approaches. The shape of the M_T spectra shall

[1] In the appendix one can find a derivation of the operator C, which performs such a transformation

be analyzed for this purpose. Therefore normalized and logarithmic plots will be used.
The results show, that there is the same impact of a varying mediator mass on the M_T spectrum for each approach. In fig.4.1 one can see the M_T spectrum for each mediator mass and approach for the case $\xi = -1$, where it is apparent that the shapes are very similar for both approaches. For lower mediator masses the cross section scales higher. Since the plots

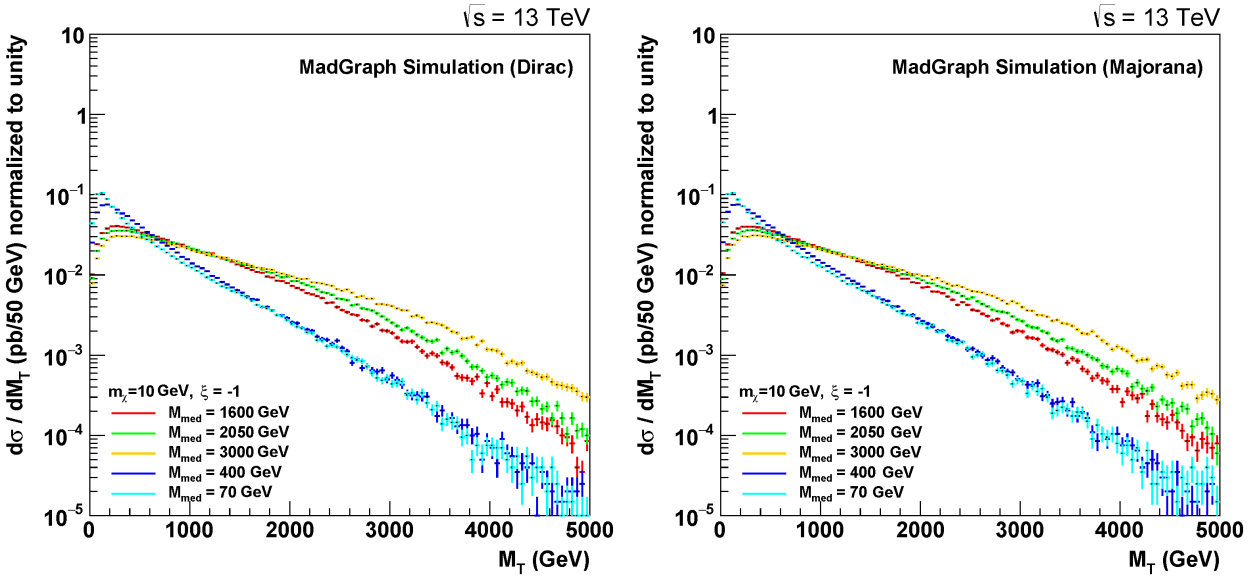

Figure 4.1: logarithmic plot of M_T with $\xi = -1$.Left: Dirac. Right: Majorana.

in fig.4.1 are logarithmic plots, this can be seen better in fig.4.2. Additionally it was found that this behavior is valid for the Dirac approach as well as the Majorana approach. Here one can again see the similarity of the shapes of both approaches. The described behavior

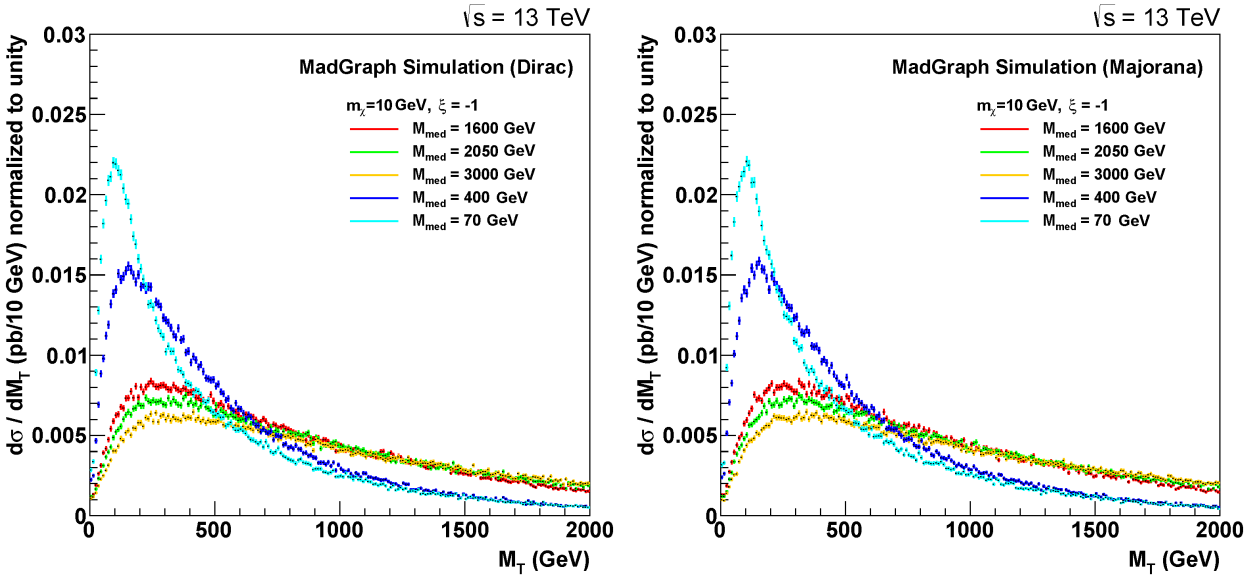

Figure 4.2: normalized plot of M_T with $\xi = -1$.Left: Dirac. Right: Majorana.

appears also for the other two cases of ξ. In fig.4.3 this result is presented for the Majorana model[2].
The fact that the cross section scales higher at low mediator masses is something one would

[2]The plots for the Dirac case can be found in the appendix

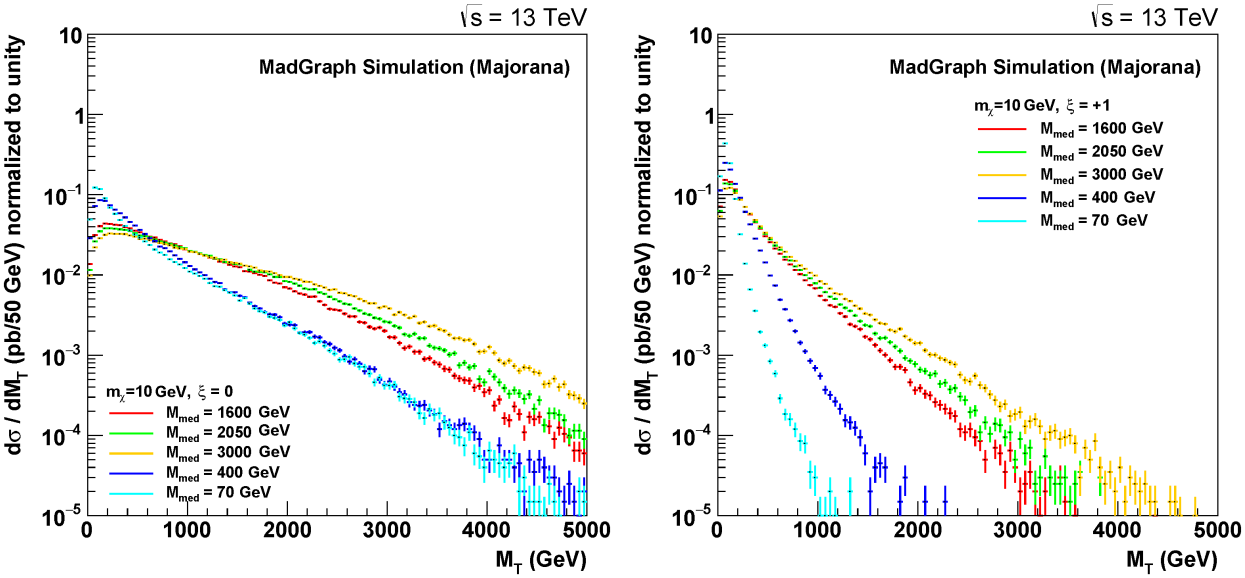

Figure 4.3: logarithmic plot of M_T for the Majorana approach. Left: $\xi = 0$. Right: $\xi = +1$

expect. The dependency of the cross section is

$$\begin{aligned} \sigma &\propto \frac{g_\chi^2 \cdot s}{(s - M_{med})^2 + s\Gamma_{med}^2} \\ &\propto \frac{g_\chi^2 \cdot s}{(s - M_{med})^2 + M_{med}^2 \cdot \frac{s}{64\pi^2}}, \end{aligned} \tag{4.1.4}$$

since $\Gamma_{med} = \frac{M_{med}}{8\pi}$. This dependency explains the observed behavior of the cross section. The analysis of the sensitivity for changes in m_χ yields the same results. The parameter was varied between $m_\chi \in \{10\text{ GeV}, 100\text{ GeV}, 500\text{ GeV}, 1300\text{ GeV}, 2499\text{ GeV}\}$. The mediator mass is fixed to $M_{med} = 5000$ GeV. The graphs in fig.4.4 show the M_T spectra for the different choices of m_χ for each approach. One again finds a strong similarity regarding the impact of

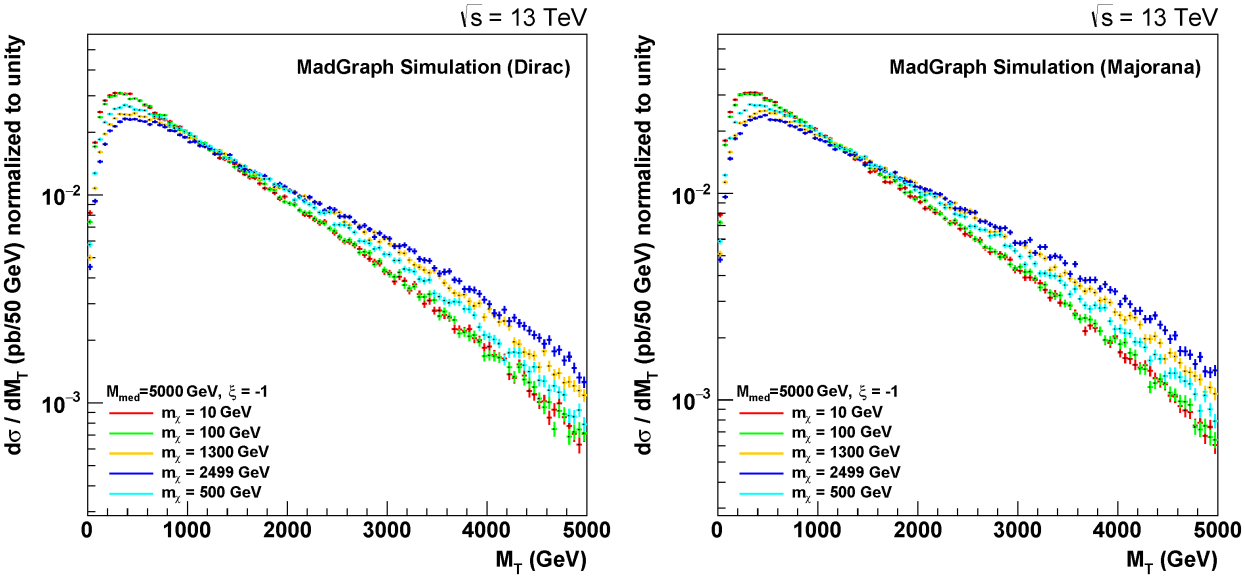

Figure 4.4: logarithmic plot of M_T with $\xi = -1$. Left: Dirac. Right: Majorana.

the variation of the considered parameter m_χ on the M_T spectra for each approach. Here,

too one can see a strong similarity between the shapes of both approaches for the several choices of m_χ. For lower DM masses the cross section is larger, but they do not scale it as high as low mediator masses do. This can be seen in fig.4.5. One can see the same behavior

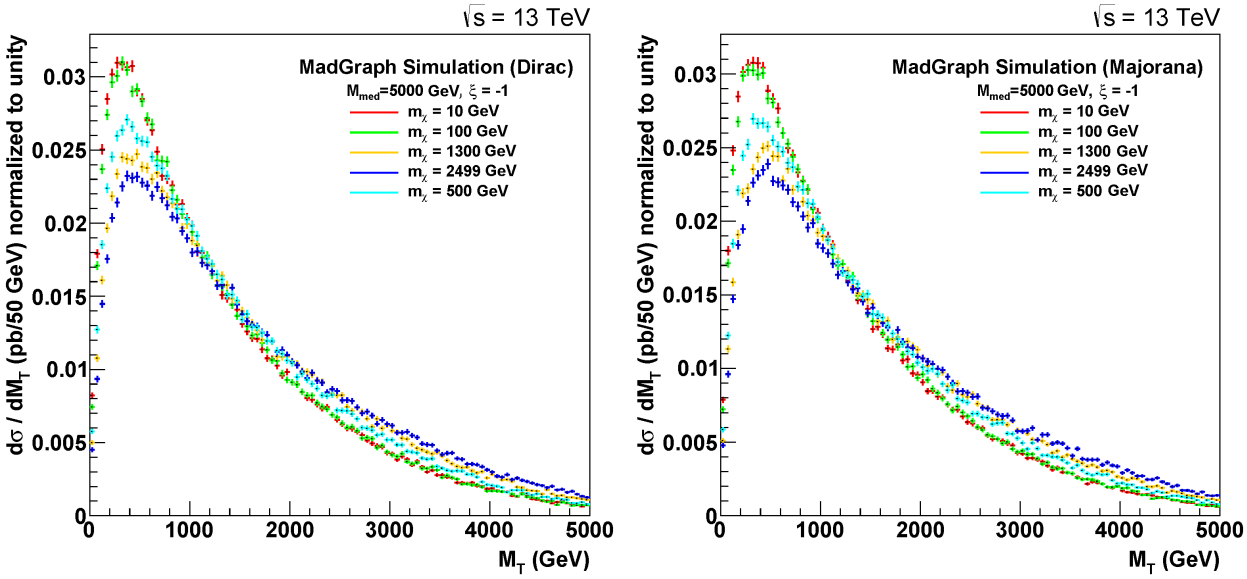

Figure 4.5: normalized plot of M_T with $\xi = -1$. Left: Dirac. Right: Majorana.

for the other cases of ξ (see fig.4.6).

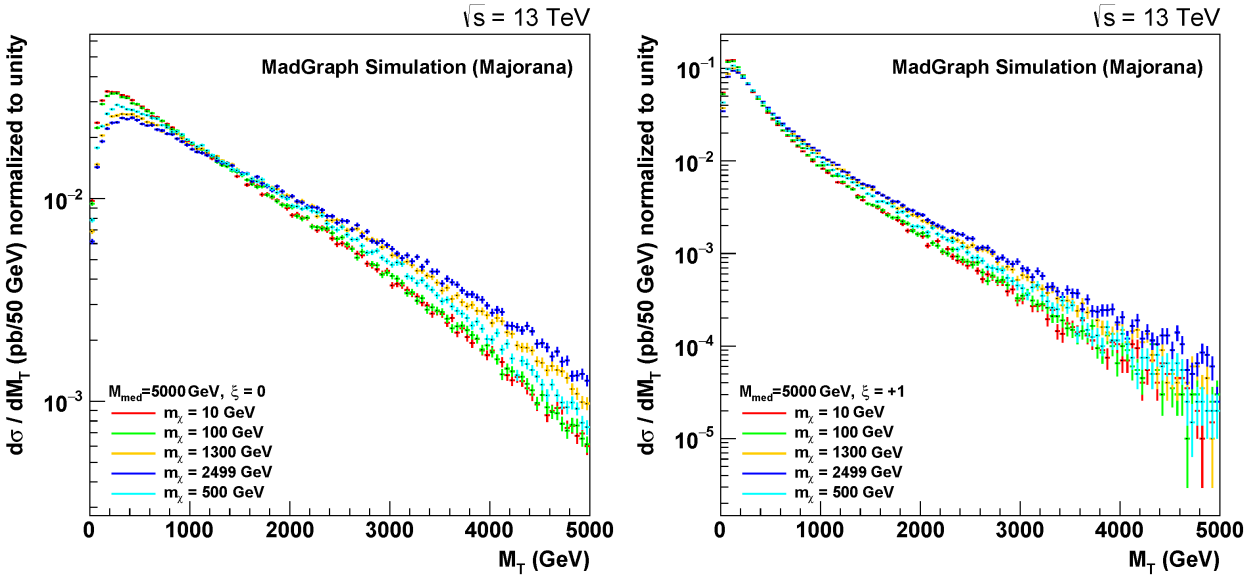

Figure 4.6: logarithmic plot of M_T for the Majorana approach. Left: $\xi = 0$. Right: $\xi = +1$

In fig.4.2 and 4.5 a strong similarity between the shapes of the M_T spectra of either Majorana or Dirac DM was found. A direct comparison of these two approaches within one plot can be seen in fig.4.7. The normalized plot shows that there is no difference in the shape at all, while it can be seen in the non-normalized plot, that there is a factor of two of difference for the cross section between the two approaches. A table of the σ that the MadGraph simulations calculated (see table 4.1) shall confirm this factor, which is due to the fact, that in the Majorana case one has identical particles. The combinatorics of such particles differ from those of Dirac fermions [10, 11, 13].

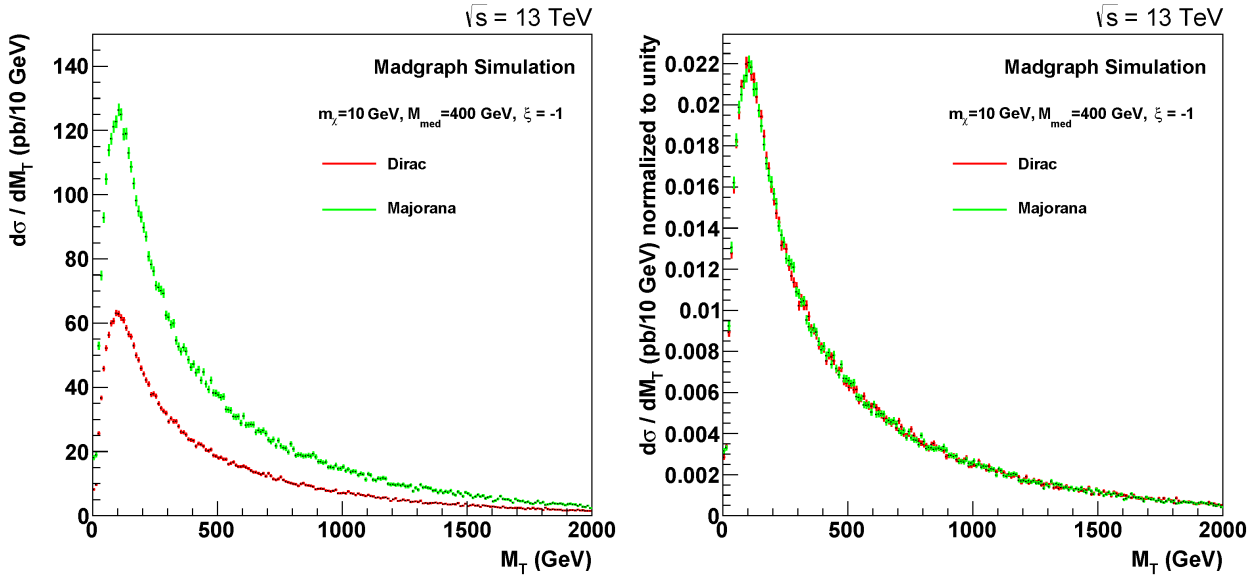

Figure 4.7: comparison of Dirac and Majorana M_T spectrum for $\xi = -1$ and M_{med}=400 GeV. Left: non-normalized graph for Majorana and Dirac. Right: normalized graph for Majorana and Dirac.

	$\xi = +1$		
M_{med}/GeV	σ_M/pb	σ_D/pb	σ_M/σ_D
70	405.24 ± 0.27	202.40 ± 0.13	2.002 ± 0.002
1600	0.337943 ± 0.000175	0.168933 ± 0.000092	2.000 ± 0.002
3000	0.015049 ± 0.000008	0.007518 ± 0.000004	2.002 ± 0.002

	$\xi = 0$		
M_{med}/GeV	σ_M/pb	σ_D/pb	σ_M/σ_D
70	1534.76 ± 0.92	769.21 ± 0.45	1.995 ± 0.002
1600	1.305404 ± 0.000872	0.652477 ± 0.000428	2.001 ± 0.002
3000	0.063214 ± 0.000043	0.031614 ± 0.000022	2.000 ± 0.002

	$\xi = -1$		
M_{med}/GeV	σ_M/pb	σ_D/pb	σ_M/σ_D
70	5726.95 ± 3.25	2869.34 ± 1.74	1.996 ± 0.002
1600	4.8834 ± 0.0032	2.4431 ± 0.0017	1.999 ± 0.002
3000	0.2378 ± 0.0002	0.1188 ± 0.0001	2.002 ± 0.002

Table 4.1: Table of cross sections for the different cases of ξ

The summary of the results of this section is, that there is no difference for the kinematics beside a two times larger cross section, if one uses Majorana DM over Dirac DM. For the sake of completeness the angular distributions of each approach for one particular case were also plotted (see fig.4.8), since these are important quantities for the kinematics of a process. The results confirm the previous insights, as one also has no difference between the two approaches for these distributions.
For further analyses the Majorana approach will be used. In some cases there will also be the comparison to the Dirac approach again.

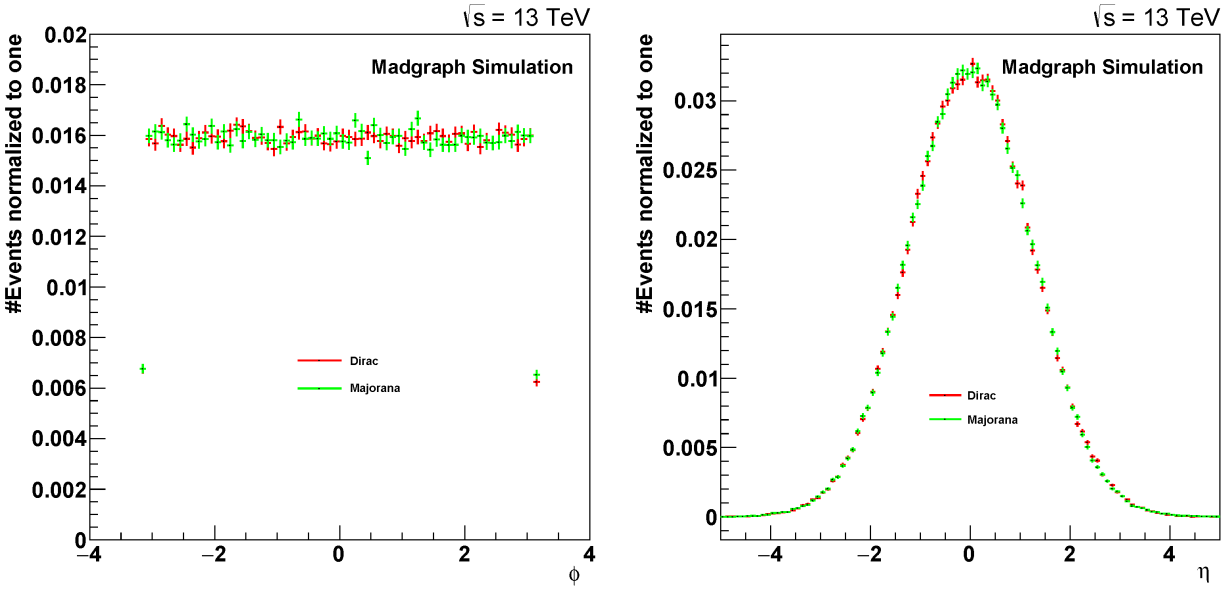

Figure 4.8: angular distributions for $\xi = -1$, $M_{med} = 400$ GeV and $m_\chi = 10$ GeV

4.2 Non-Integer Coupling

4.2.1 Motivation

A common way to analyze new physics is to assign theoretical elements, which already have proven their validity, to the unknown new mechanism or physical incident. In this section such an assignment will be made, regarding the coupling structure of the mediator V_{med}.
It will be analyzed, if assuming a coupling structure between the mediator and quarks, like the photon has it when it couples to quarks, leads to any remarkable results. Since the photon is massless and thus does not decay, one could initially refuse such an assumption. But in this analysis the point of interest are rather the coupling constants g_u and g_d. The values of these constants will be set to non-integer numbers like in case of the photon coupling to quarks.
Since up or down quarks carry an electrical charge of $+\frac{2}{3}e$ or $-\frac{1}{3}e$, only these values will be used in this rather short analysis. The parameter space thus is given by $g_{u,d} \in \{\pm\frac{2}{3}, \mp\frac{1}{3}\}$. The values for the mediator and dark matter masses will be fixed to $m_\chi = 10$ GeV and M_{med} = 400 GeV. As it was mentioned earlier, in this section the coupling constants $g_{u,d}$ will be used instead of the parameter ξ.

Results

In section 2.3.3 the interference cases of the mono-lepton channel were introduced. When this interference was first introduced in [8], only integer values for the coupling constants were considered. This analysis has shown that one can produce the same cases of either destructive of constructive interference with non-integer values, too (see 4.9).
Furthermore one can see, that the interference cases do only depend on the relative sign between the couplings g_u and g_d. A relative minus sign between this constants causes constructive interference, while the same sign for both constants correspondents to destructive interference. A deeper look into the cross section's dependency on the matrix elements $\mathcal{M}_{u,d}$ can explain this behavior:
It was already stated that

$$\sigma \propto |g_u\mathcal{M}_u + g_d\mathcal{M}_d|^2 \quad . \tag{4.2.1}$$

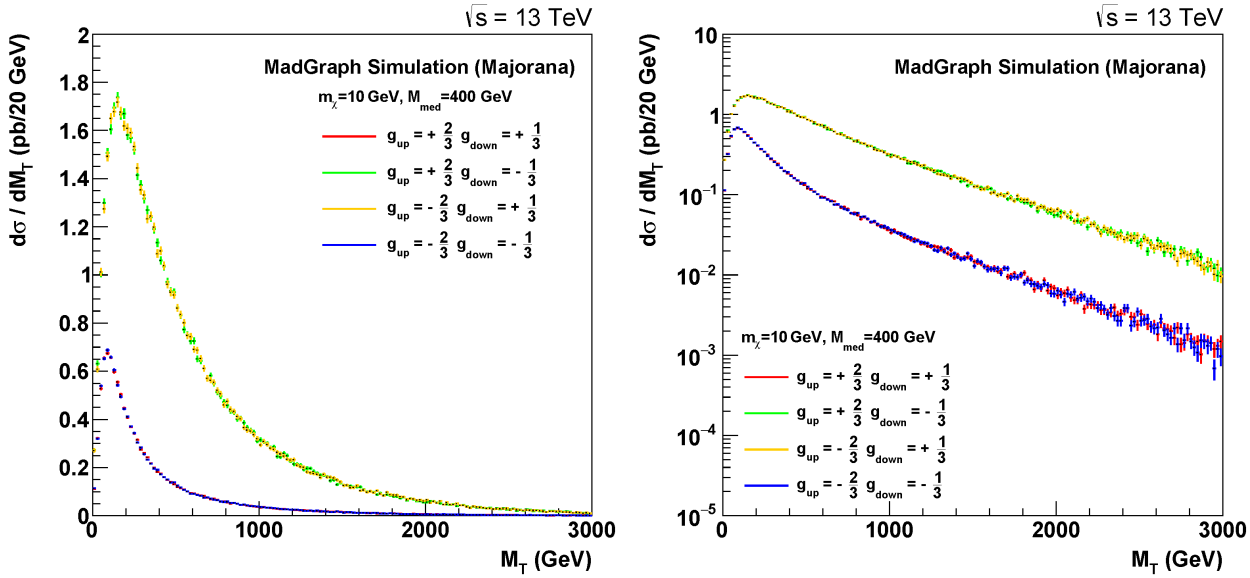

Figure 4.9: non-logarithmic (left) and logarithmic (right) M_T spectra

A further execution of this equation gives

$$\sigma \propto g_u^2|\mathcal{M}_u|^2 + g_d^2|\mathcal{M}_d|^2 + g_u g_d \cdot \mathrm{Re}\left(\mathcal{M}_u^* \mathcal{M}_d + \mathcal{M}_d^* \mathcal{M}_u\right). \tag{4.2.2}$$

It is easy to see, that the cross section scales different for various couplings $g_{u,d}$. Furthermore the rate of interference does also depend on both coupling factors, since the last term in the upper equation describes it. One also understands, that the sign of the interference term has to be negative, since a different sign of g_u and g_d produces constructive interference and vice versa.
Summarized this short analysis has shown, that the interference cases in the mono-lepton channel can also be produced with non-integer values for the couplings.

4.3 Validity of ξ

4.3.1 Theoretical Basics

In this section the parameter ξ with it being defined like in section 2.3.3 is going to be discussed. There, it had been declared to be the coupling to down quarks and therefore was defined like

$$V_\mu \bar{u}\gamma^\mu\gamma_5 u \quad + \quad \xi \cdot \quad V_\mu \bar{d}\gamma^\mu\gamma_5 d, \tag{4.3.1}$$

where the coupling to up quarks is set to one.
The variation of this parameter within $\xi \in \{-1, 0, 1\}$ causes a huge impact on the cross section. Such a behavior has already been shown in the previous section and is also illustrated in figure 4.10.
One interpretation of this behavior is to describe it as cases of different interferences. Such an explanation arises from the cross section's dependency on the matrix element. It was already found, that

$$\sigma \propto g_u^2|\mathcal{M}_u|^2 + g_d^2|\mathcal{M}_d|^2 + \underbrace{g_u g_d \cdot \mathrm{Re}\left(\mathcal{M}_u^* \mathcal{M}_d + \mathcal{M}_d^* \mathcal{M}_u\right)}_{\text{interference term}}. \tag{4.3.2}$$

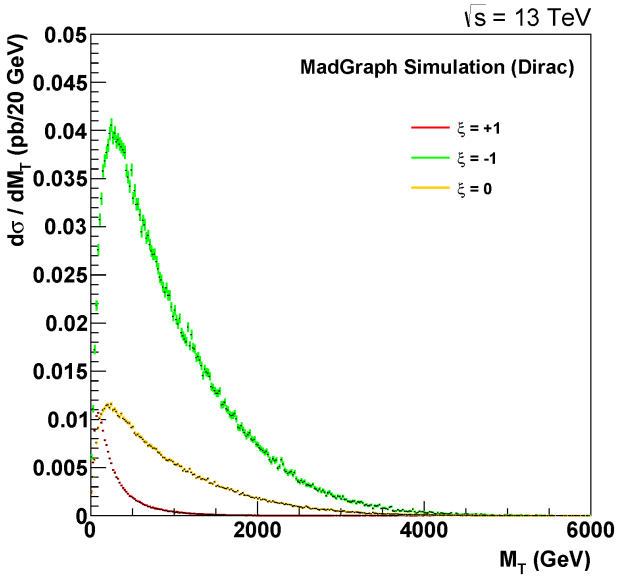

Figure 4.10: Interference behavior for different ξ with $M_{med} = 1600$ GeV and $m_\chi = 10$ GeV

what in with the definition of ξ is written as

$$\sigma \propto |\mathcal{M}_u|^2 + \xi^2 |\mathcal{M}_d|^2 + \underbrace{\xi \cdot \mathrm{Re}\left(\mathcal{M}_u^* \mathcal{M}_d + \mathcal{M}_d^* \mathcal{M}_u\right)}_{\text{interference term}}. \tag{4.3.3}$$

This interpretation was first used in [8], where an EFT for the same process as this work investigates was analyzed.
The validity of such an approach is of great importance. Due to the much lower cross section for the destructive interference case, one also has a smaller sensitivity and needs to worry about a too strong background or too weak signal. Therefore reference [7] has gained great attention. In this paper the authors show, that for an EFT the case $\xi = -1, 0$ are restricted. The argumentation of this paper is as follows:
The starting point of argumentation is, that for such an EFT the operator which is used to describe the interaction of the mono lepton channel violated the gauge invariance of the $SU(2)_L$ symmetry, if one used different couplings to up and down quarks.
Using this $SU(2)_L$ violating operator would lead to the violation of the so called Ward identity. The Ward identity is very important for gauge theories. It can be seen as the quantum field theoretical analogon of Noether's theorem, since every symmetry of the theory has such an identity. The satisfaction of this identity is connected to the guarantee of the respective gauge invariance [18, 22, 23]. For the mono-lepton channel the authors of the discussed paper have derived such a Ward identity for the $SU(2)_L$ symmetry of an EFT. The result is

$$\mathcal{M}^\alpha \epsilon_\alpha^L \approx \frac{q_\alpha}{m_W} \mathcal{M}^\alpha(q) = i\mathcal{M}(\phi^+(q)) \approx 0, \tag{4.3.4}$$

where ϵ_α^L is the longitudinal polarization vector of the W boson. The sum over the amplitudes of the the mono-W decay are given by

$$q_\alpha \mathcal{M}^\alpha = \frac{g_W}{\Lambda} \left[\bar{v}(p_2)(1-\xi)\gamma^\mu \frac{P_L}{\sqrt{2}} u(p_1)\right] \left[\bar{u}(k_1)\gamma_\mu v(k_2)\right]. \tag{4.3.5}$$

The Ward identity requires this term to be zero. Since this is obviously just the case if $\xi = +1$, the authors use this to restrict the other two values for ξ, or even more generally

every combination of unequal couplings to up and down quarks.
The case of constructive interference, where the $SU(2)_L$ Ward identity is thus violated, scaled so high because of the Ward identity's violation causing an increased production of longitudinally polarized W bosons. The concrete cross section for the case of constructive interference ($\xi = -1$) is calculated in the paper and it is shown, that one has an additional term in the cross section, which grows with the partonic center of mass energy, like

$$\sigma \propto \frac{\hat{s}}{m_W^2}. \tag{4.3.6}$$

Here the partonic center of mass energy is denoted as $\hat{s}$ in order to avoid confusion with the center of mass energy $\sqrt{s}$ of the proton system. This additional term in the cross section leads to the violation of unitarity for $\hat{s} \gg m_W^2$. For $\sqrt{s} = 13$ TeV this condition clearly is satisfied and one thus has problems at high $\hat{s}$. One explicit consequence of this violation is a very strong divergence of the parton level cross section.
Summarized, this paper makes the following argumentation:

- for $\xi \neq 1$ the $SU(2)_L$ gauge invariance is violated and thus the respective Ward identity is broken
- in this cases more longitudinally W are produced as a consequence of the above mentioned violation
- at high energies there is a very strong divergence of the parton level σ, which violates unitarity

At this point a more general question of whether the upper mentioned violations should be arranged with, since the EFT as well as the simplified model are toy models, could be asked. However, this thesis aims to make a less general discussion. It will be investigated whether the results of the above mentioned paper are applicable to a simplified model, as well. Since there is a mediator implementation in this model, and thus there is a different intermediate state, this should be well motivated. The strategy of analysis is to check the behavior of the three main arguments of the authors of [7]. Therefore the following aspects will be investigated:

- check the polarization of the W boson in the simplified model for several mediator masses
- make a plot of the partonic level cross section and analyze it, also for various mediator masses
- check if the simplified model is gauge invariant for the cases $\xi \neq 1$

These steps are ordered chronologically with respect to the investigations that were done. This decision was made in order to show the development of the whole analysis.
In order to understand the analysis of the W boson's polarization a short derivation of the the three possible polarizations for a W will be made. Let us start with the matrix element $\mathcal{M}$ for the mono leptonic W decay:

$$\mathcal{M} = \frac{g_W}{\sqrt{2}} \epsilon_\mu(p_1) \underbrace{\bar{u}(p_3)\gamma^\mu \frac{1}{2}(1-\gamma^5)\nu(p_4)}_{j^\mu}, \tag{4.3.7}$$

where g_W is the constant for the weak interaction, ϵ_μ is the polarization vector, j^μ is the weak charged current, p_1 is the W boson's momentum and p_3 and p_4 are the leptons and

neutrinos momenta. It is worked in the rest frame of the W boson, and therefore j^μ becomes

$$j^\mu = 2E \begin{pmatrix} 0 \\ -\cos\theta \\ -i \\ \sin\theta \end{pmatrix} = m_W \begin{pmatrix} 0 \\ -\cos\theta \\ -i \\ \sin\theta \end{pmatrix}, \tag{4.3.8}$$

since in this frame one finds $E = E_l = E_\nu = \frac{m_W}{2}$. Here, θ is the angle between the lepton and the W boson (see figure 4.11)[3]. The three different polarizations[4] are described by these polarization vectors:

$$\epsilon^\mu_{T_+} = \frac{1}{\sqrt{2}} \begin{pmatrix} 0 \\ 1 \\ -i \\ 0 \end{pmatrix} \quad \epsilon^\mu_{T_-} = -\frac{1}{\sqrt{2}} \begin{pmatrix} 0 \\ 1 \\ i \\ 0 \end{pmatrix} \quad \epsilon^\mu_L = \begin{pmatrix} 0 \\ 0 \\ 0 \\ 1 \end{pmatrix} \tag{4.3.9}$$

Plugging these two results into equation 4.3.7 let's one calculate the respective matrix element and one finds

$$\mathcal{M}_{T_\pm} = \frac{g_W}{\sqrt{2}} \epsilon^{T_\pm}_\mu j^\mu = \pm \frac{g_W m_W}{2} (0, -1, \pm i, 0) \begin{pmatrix} 0 \\ -\cos\theta \\ -i \\ \sin\theta \end{pmatrix} = \pm \frac{g_W m_W}{2} (\cos\theta \pm 1), \tag{4.3.10}$$

for transverse polarization and

$$\mathcal{M}_L = \frac{g_W}{\sqrt{2}} \epsilon^L_\mu j^\mu = \frac{g_W m_W}{\sqrt{2}} (0, 0, 0, -1) \begin{pmatrix} 0 \\ -\cos\theta \\ -i \\ \sin\theta \end{pmatrix} = -\frac{g_W m_W}{\sqrt{2}} \sin\theta \tag{4.3.11}$$

for longitudinal polarization. Calculating the absolute values gives finally [29]

$$\begin{aligned} |\mathcal{M}_{T_\pm}|^2 &= \frac{g_W^2 m_W^2}{4} (1 \pm \cos\theta)^2 \\ |\mathcal{M}_L|^2 &= \frac{g_W^2 m_W^2}{2} \sin^2\theta. \end{aligned} \tag{4.3.12}$$

The figure below shall illustrate each polarization (the scaling factors g_W^2 and m_W^2 are set to 1).
Since the other analysis steps are rather straight forward, the necessary information will be mentioned while presenting the results.

4.3.2 Results

In order to get the right angle, a Lorentz boost was performed into the W boson's rest frame. It was necessary to find a way to quantify how big the rate of each W polarization is. This was solved by fitting a function of the form

$$f(\theta) = \frac{a}{4} (1 + \cos\theta)^2 + \frac{b}{2} \sin^2\theta + \frac{c}{4} (1 - \cos\theta)^2 \tag{4.3.13}$$

[3] In the results section this angle will also be referred to as $\Delta\phi$

[4] Since the W is a boson, it is a spin 1 particle. Therefore its spin can take the values $S_z = \pm 1, 0$. The cases of $S_z = \pm 1$ correspond to transversal polarization, whereas the case with $S_z = 0$ corresponds to longitudinal polarization.

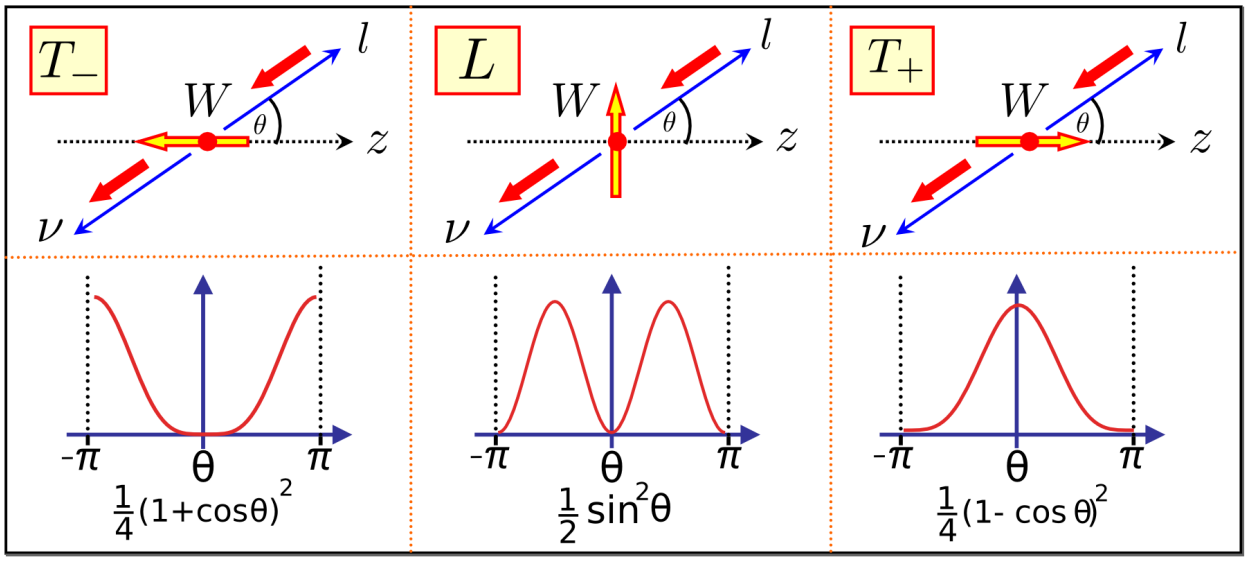

Figure 4.11: polarizations of the W boson (adapted from [26, 29])

to the results, with a,b and c being parameters. To get the rate of each polarization, each parameter was normalized and thus one gets

$$T_+ = \frac{a}{N} \quad L = \frac{b}{N} \quad T_- = \frac{c}{N}, \quad \text{with} \quad N = a + b + c \tag{4.3.14}$$

to be the rate for each polarization. For a better depiction of the results' polarization fractions, the fitted functions were also plotted into the canvas. The scaling factors g_W^2 and m_W^2 were ignored.
In the figures 4.12-4.14 one can see the behavior for each cases and various mediator masses. The results for $\xi = 0$ will not be presented, since this case shows the same results as $\xi = -1$,

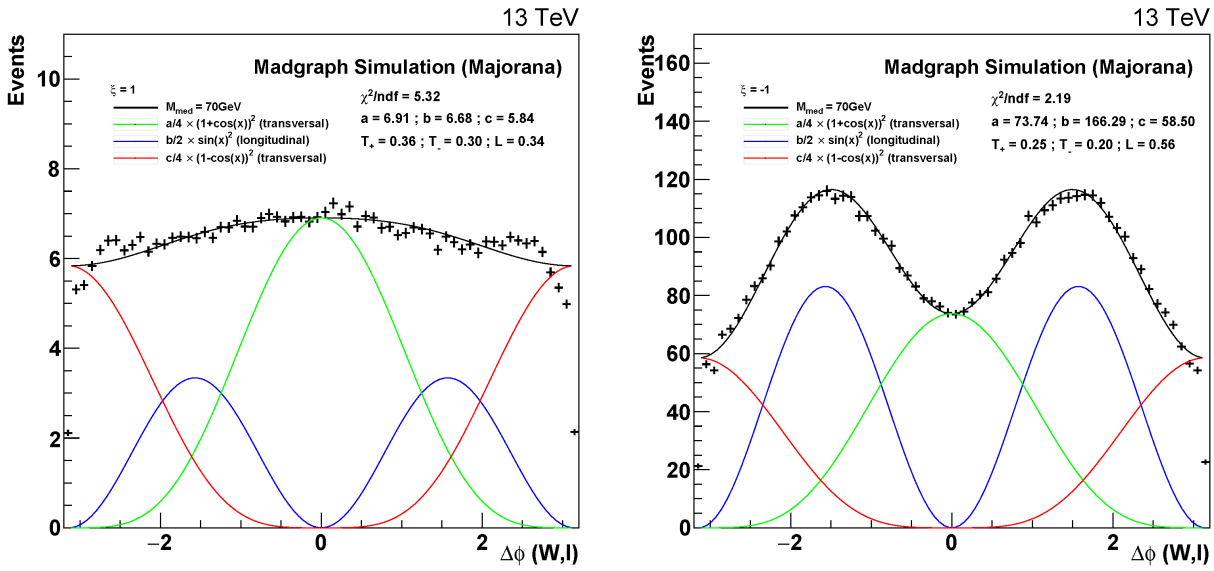

Figure 4.12: Comparison for $M_{med} = 70$ GeV. Left: $\xi = +1$. Right: $\xi = -1$

except having a lower cross section. It was furthermore decided to show three values of M_{med}, namely $M_{med} \in \{70 \text{ GeV}, 1600 \text{ GeV}, 3000 \text{ GeV}\}$. The plots show, that there is less

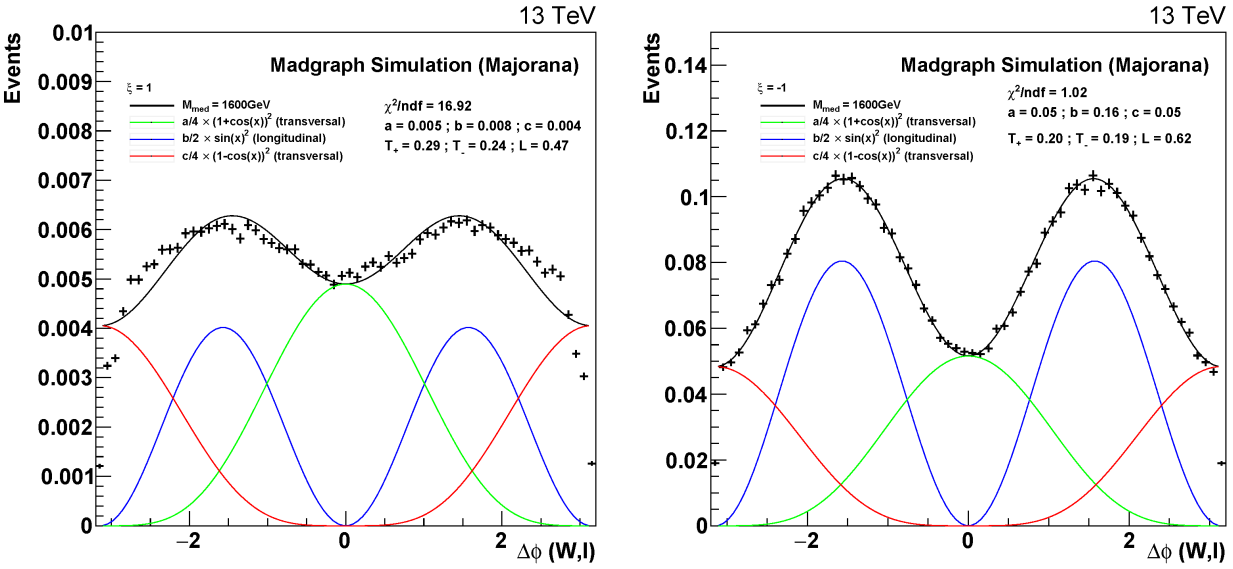

Figure 4.13: Comparison for $M_{med} = 1600$ GeV. Left: $\xi = +1$. Right: $\xi = -1$

longitudinal polarization for the case $\xi = +1$, when decreasing the mediator mass. Especially for $M_{med} = 70$ GeV the rate of transverse polarization is higher than the rate for longitudinal polarization ($\approx$35%). For every value of M_{med} the longitudinal polarization is less than the transverse, but this difference shrinks for higher mediator masses. For $\xi = -1$ by contrast,

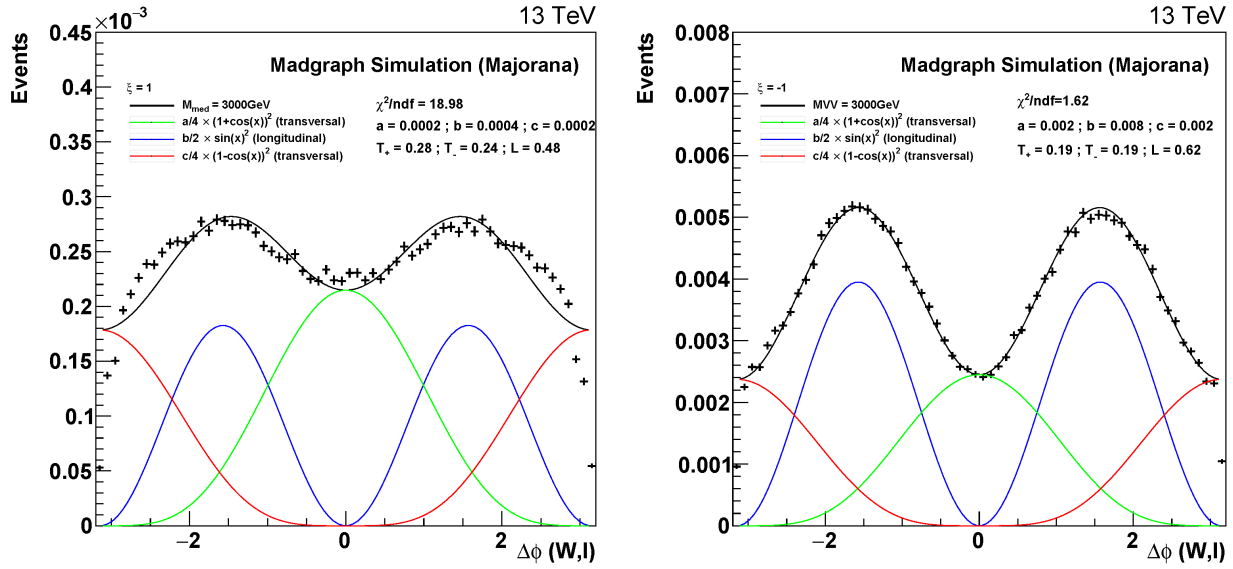

Figure 4.14: Comparison for $M_{med} = 3000$ GeV. Left: $\xi = +1$. Right: $\xi = -1$

the longitudinal polarization fraction is always greater ($\approx$60%). Nevertheless, one can see that for $M_{med} = 70$ GeV the rate for longitudinal polarization shrinks a little ($\approx$56%). It was checked if there is a dependency of the W's polarization on the polarization of the initial quarks. The results, which can be found in the appendix, have shown, that there is no such dependency.

A comparison to the W polarization of an EFT shows, that this analysis does not give an access to the question, if the results of the above mentioned paper are applicable to a simplified model as well, at all. As fig.4.15 shows, there is no difference in the rate of

longitudinal or transverse polarization if one changes the parameter ξ's value. This means, that the restriction on longitudinally polarized W, was rather an energetic argument in the above mentioned paper. It was not stated, that the rate for the production of differently polarized W bosons changes for the case $\xi \neq 1$ but that one has more longitudinally polarized W at all, due to the higher cross section. A production of so much longitudinally polarized W bosons in the intermediate state leads to the violation of unitarity and the divergence of the parton level cross section and thus is considered to be *unphysical* [7].

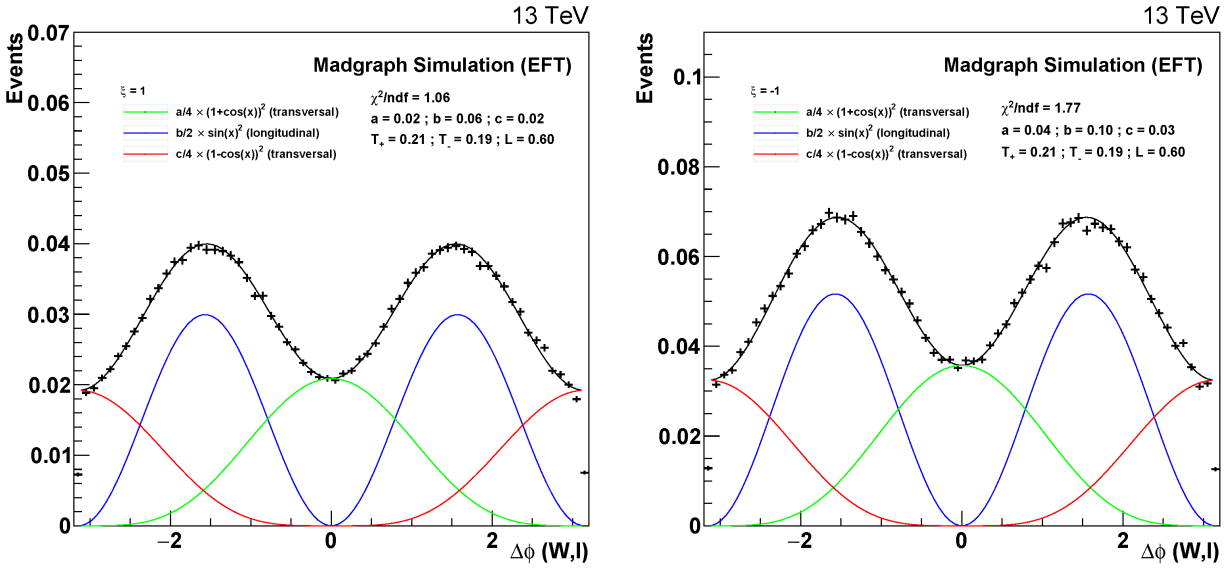

Figure 4.15: Comparison for an EFT with $m_\chi = 10$ GeV. Left: $\xi = +1$. Right: $\xi = -1$

Nevertheless, these results can be used to explain the behavior depicted in figures 4.12-4.14. As the EFT is valid for very large mediator masses, both results match to each other. In figure 4.15 one sees, that the rate for each polarization does not change at all for the EFT, if one changes the value of ξ. For the simplified model it was found, that the difference between the two cases of ξ is shrinking for higher mediator masses. In the limit of a very high mass the simplified model will yield the same results as the EFT.
Since the analysis above does not provide an access to the question, it will be continued with the second part of this investigation. As it was stated above, here the same parton level cross section plots will be made as the theorists have done it in their paper. For these plots the *parton distribution functions* (pdfs) had to be unfolded in order to get the cross section on the y-axis. A parton distribution function gives one the probability for a parton to carry a certain amount of the energy of the hadron, whose constituent the parton itself is. Such a distribution function is needed, since the simple assumption of hadrons consisting out of three quarks is not precise enough. In fact these three quarks are the so called *valence quarks* and there are additional gluons and so called *sea quarks* within a hadron.
This unfolding of the pdfs takes the following form:

$$\sigma\left(\sqrt{\hat{s}}\right) = \frac{1}{f_1(x_1, Q) \cdot f_2(x_2, Q)} \cdot \frac{\sigma_{total}}{\#Events}. \tag{4.3.15}$$

Here, $\sqrt{\hat{s}}$ is defined as $\sqrt{\hat{s}} = |p_z(q_1)| + |p_z(q_2)|$ and σ_{total} is the cross section of the whole simulation. This unfolding is done for every event and can therefore be understood as an integration over the phasespace.
A problem arises, for energies above at about a third of the proton system's center of mass

energy $\sqrt{s}$. Since one has rather low statistics for such high energies, the errors on the respective cross sections are very high. This distorts the results and it was therefore decided to plot the results up to $\sqrt{\hat{s}} \approx \frac{\sqrt{s}}{3}$.
For these plots it was decided to look at five different mediator masses again. This time the mediator mass varies between $M_{med} \in \{70\text{ GeV}, 400\text{ GeV}, 1600\text{ GeV}, 2025\text{ GeV}, 3000\text{ GeV}\}$ and m_χ is again fixed to 10 GeV. The results will only be shown for $M_{med} \in \{70\text{ GeV}, 400\text{ GeV}, 3000\text{ GeV}\}$. The considered cases of ξ are $\xi = \pm 1$. Such plots are made for every model used in this analysis: the simplified model with either Dirac or Majorana DM and the EFT.
The results are shown in figure 4.16-4.18. One can see, that there is a difference between the EFT and the simplified models, for both cases of ξ. Especially for $\xi = +1$ one has a very different slope. There is a clear peak over the mass of both mediators $M_{med} + m_W$.

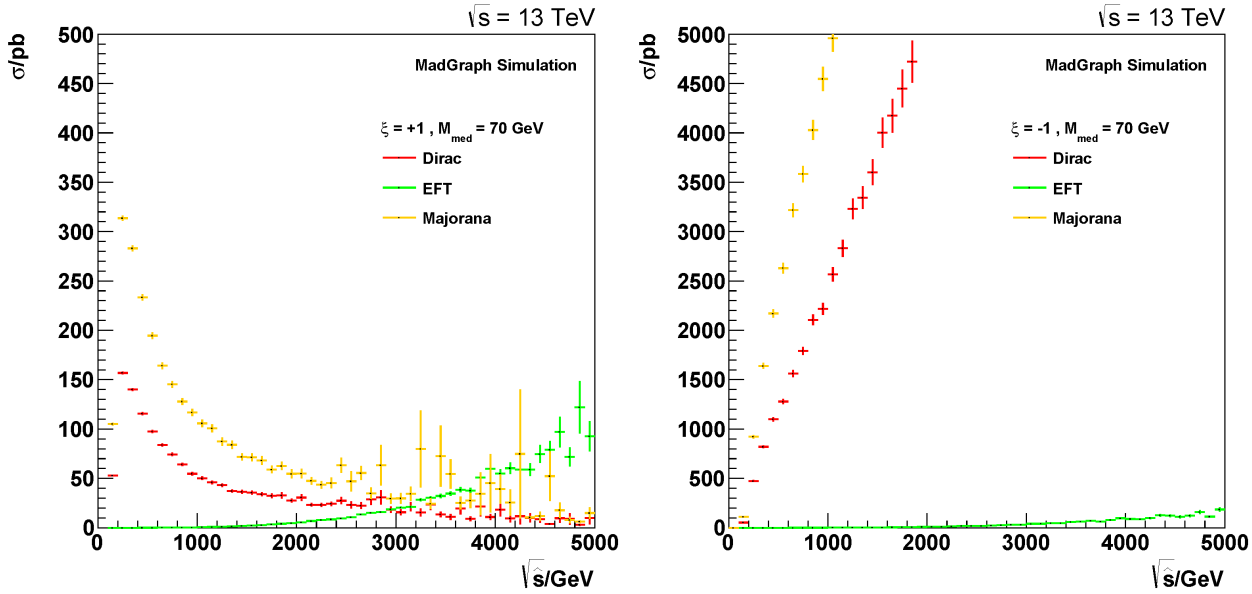

Figure 4.16: Parton level σ for $M_{med} = 70$ GeV. Left: $\xi = +1$. Right: $\xi = -1$

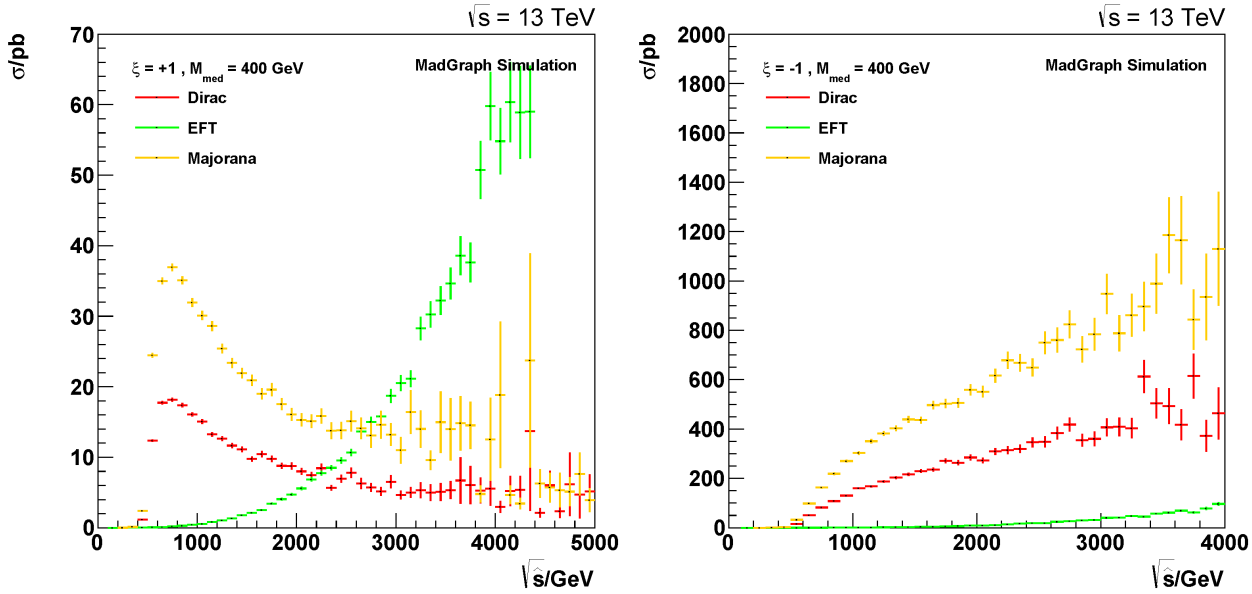

Figure 4.17: Parton level σ for $M_{med} = 400$ GeV. Left: $\xi = +1$. Right: $\xi = -1$

More interesting for this analysis is the difference for $\xi = -1$. One can see that the EFT grows much stronger with $\sqrt{\hat{s}}$ than the simplified model does, when high mediator masses are considered. There even is a general difference between the slopes. In [7] it was mentioned, that for this case the EFT would grow like $\sigma \propto \hat{s}$. In point of fact, such a behavior can be seen in fig.4.18 in the right plot, since the EFT is clearly growing like an exponential function. For the simplified model in contrast, one can see that it rather follows a differ-

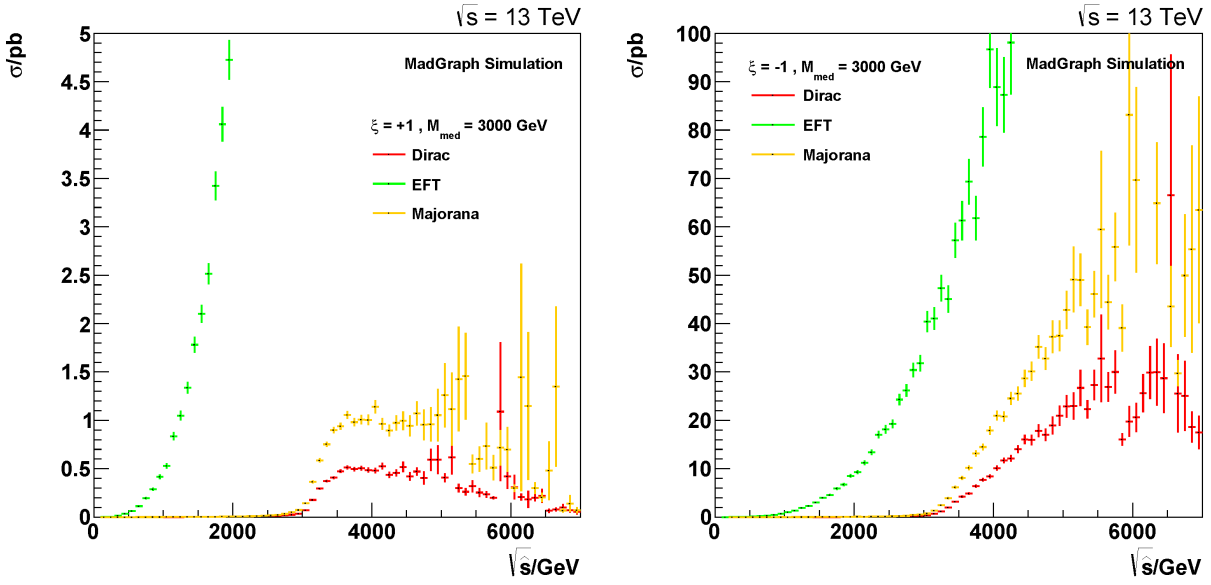

Figure 4.18: Parton level σ for $M_{med} = 3000$ GeV. Left: $\xi = +1$. Right: $\xi = -1$

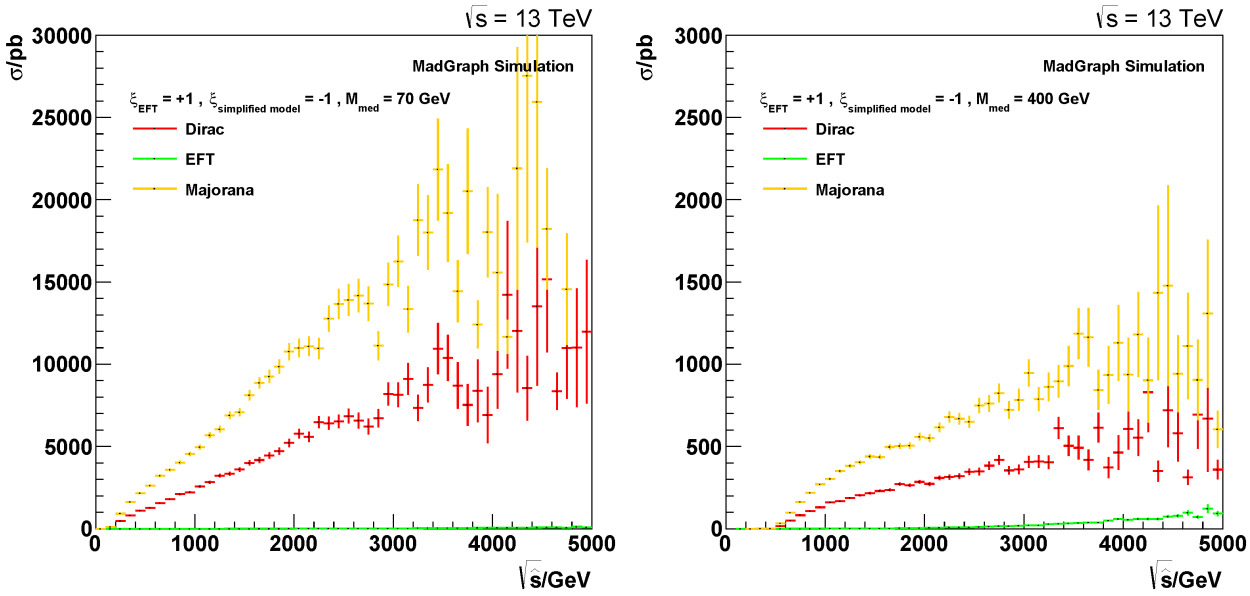

Figure 4.19: Comparison with ξ_{EFT}=+1 and $\xi_{\text{simplified model}}$=-1. Left: $M_{med} = 70$ GeV. Right: $M_{med} = 400$ GeV.

ent functional dependency on $\sqrt{\hat{s}}$. The simplified model is rather growing like a hyperbolic function, especially at low mediator masses, what could indicate a dependency like $\sigma \propto \hat{s}^{\frac{1}{n}}$, where $n > 2$, since there is $\sqrt{\hat{s}}$ on the x-axis. This is some evidence for a fundamentally different behavior of σ at high energies. Although there is a much stronger growth for lower mediator masses (see fig. 4.16), it could therefore not diverge as strong as the EFT at very

high energies. Additionally the growth always begins at the mass of the intermediate state $M_{med}+m_W$, what particularly for high mediator masses leads to a different behavior at high energies. Therefore the case $\xi = -1$ could still satisfy unitarity and gauge invariance for a simplified model in general.
Fig. 4.19-4.20 show plots, where the EFT's valid case $\xi = +1$ is compared to the simplified model's $\xi = -1$ case.
Especially for great M_{med} one sees, that the EFT's valid case is growing much stronger than the simplified model's $\xi = -1$ case (see figure 4.20). The different slope between the growth can be seen in fig.4.19 on the right. These incidents are indications for the cases $\xi \neq 1$ to be valid for sufficiently high mediator masses.
A justified question that could arise at this point is, why the simplified model shows such a different behavior even for great masses, where it should rather match to the EFT's results. Although a mass of 3000 GeV was already enough to produce about the same results for the EFT and the simplified model when the polarization was investigated, this value for M_{med} is not enough mass to produce comparable results in any account. Such a boundary on the mass of the simplified models mediator was found in [21] to be at about 7000 GeV. This nevertheless does not have to mean, that arbitrary high mediator masses will yield the same results as an EFT, since this was only shown for the cross section in [21]. The plots that are discussed here are directly connected to the intermediate state, whereas it would be more intuitive to expect a different behavior compared to an EFT even for high mediator masses.

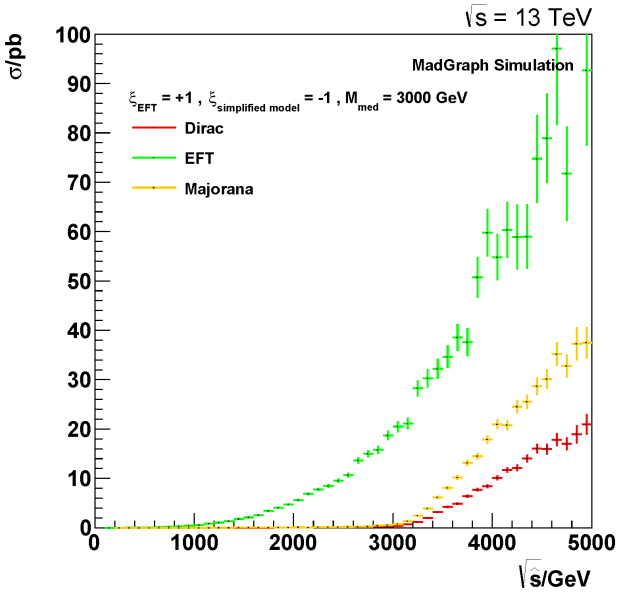

Figure 4.20: Comparison with ξ_{EFT}=+1, $\xi_{\text{simplified model}} = -1$ and $M_{med} = 3000$ GeV.

Since these results are not conclusive enough to declare the considered cases of the simplified model to be valid, a further step was taken. In a discussion with Leila Ali Cavasonza, a PhD student from the RWTH Aachen's Department for Theoretical Particle Physics and Cosmology, it was learned, that there was a possibility to check gauge invariance in MadGraph. She stated, that there was a command "*Set gauge unitary/Feynman*", which can be used in order to switch between different gauges before generating the events. The best way to check if the model is gauge invariant was using different gauges to calculate the cross section.
Such an investigation was done and the cross section for all three cases of ξ and $M_{med} \in \{50$

GeV, 400 GeV, 1000 GeV, 5000 GeV, 15000 GeV[5]} was calculated by MadGraph for each gauge with the Dirac model. The dark matter mass m_χ again was put to 10 GeV. These runs were made with 200000 Events, since it here is particularly important to merge out statistical errors. Additionally, plots of the M_T spectra were made for the purpose of comparison.
The following table, where the index U stands for unitary and F for Feynman gauge, shows the results of the cross section calculations:

	$\xi = +1$		
M_{med}/GeV	σ_U/pb	σ_F/pb	σ_U/σ_F
50	289.97 ± 0.19	290.01 ± 0.19	0.99986 ± 0.00092
400	10.716 ± 0.006	10.724 ± 0.006	0.99925 ± 0.00082
1000	0.92303 ± 0.00051	0.92202 ± 0.00050	1.00110 ± 0.00078
5000	0.0002110 ± 0.0000001	0.0002103 ± 0.0000001	1.00086 ± 0.00079

	$\xi = 0$		
M_{med}/GeV	σ_U/pb	σ_F/pb	σ_U/σ_F
50	1304.9 ± 0.7	1613.7 ± 0.9	0.80864 ± 0.00063
400	29.761 ± 0.0202	29.804 ± 0.0202	0.99856 ± 0.00096
1000	3.1555 ± 0.0022	3.1544 ± 0.0022	1.00035 ± 0.00098
5000	0.000837 ± 0.000001	0.000836 ± 0.000001	1.00094 ± 0.00102
15000	$(35.186 \pm 0.011) \cdot 10^{-7}$	$(35.140 \pm 0.012) \cdot 10^{-7}$	1.00131 ± 0.00046

	$\xi = -1$		
M_{med}/GeV	σ_U/pb	σ_F/pb	σ_U/σ_F
50	4901.8 ± 2.8	6113.1 ± 3.6	0.80185 ± 0.00066
400	108.01 ± 0.07	108.24 ± 0.07	0.99788 ± 0.00095
1000	11.668 ± 0.008	11.684 ± 0.008	0.99863 ±0.00097
5000	0.003138 ± 0.000002	0.003135 ± 0.000002	1.00115 ± 0.00093
15000	$(13.071 \pm 0.006) \cdot 10^{-6}$	$(13.071 \pm 0.006) \cdot 10^{-6}$	1.00000 ± 0.00065

Table 4.2: comparison of the cross sections calculated in different gauges

These results match to the parton level cross section plots from above. As it was seen there, the growth of the cross section was much greater for simplified models, when considering small mediator masses like $M_{med} \lesssim 400$ GeV and the cases $\xi = -1, 0$. The check of the gauge invariance gives exactly the same. One sees, that for the case $\xi = +1$ the cross section and therefore the theory itself, does not violate gauge invariance at all. Furthermore one finds, that in the cases $\xi = -1, 0$ one gets problems for low mediator masses - in this particular case at $M_{med} = 50$ GeV. For this analysis this does not only mean more evidence for a - restricted, since problems are faced at too low mediator masses - validity of $\xi \neq 1$, but does also provide a confirmation for the previous analysis and argumentation.
A comparison of the differential cross sections for $M_{med} \in \{50$ GeV, 1000 GeV, 5000 GeV$\}$ is depicted in fig.4.21 and 4.22. It can be seen, that there is a slight difference between the different gauges for low mediator masses, when one has unequal couplings to up and down quarks (see fig.4.21). For higher mediator masses one can barely discriminate between each M_T spectrum.

[5]To save calculation time the run with $\xi = +1$ and $M_{med} = 15000$ GeV was skipped, since one nevertheless does not expect violation of invariance for $\xi = +1$

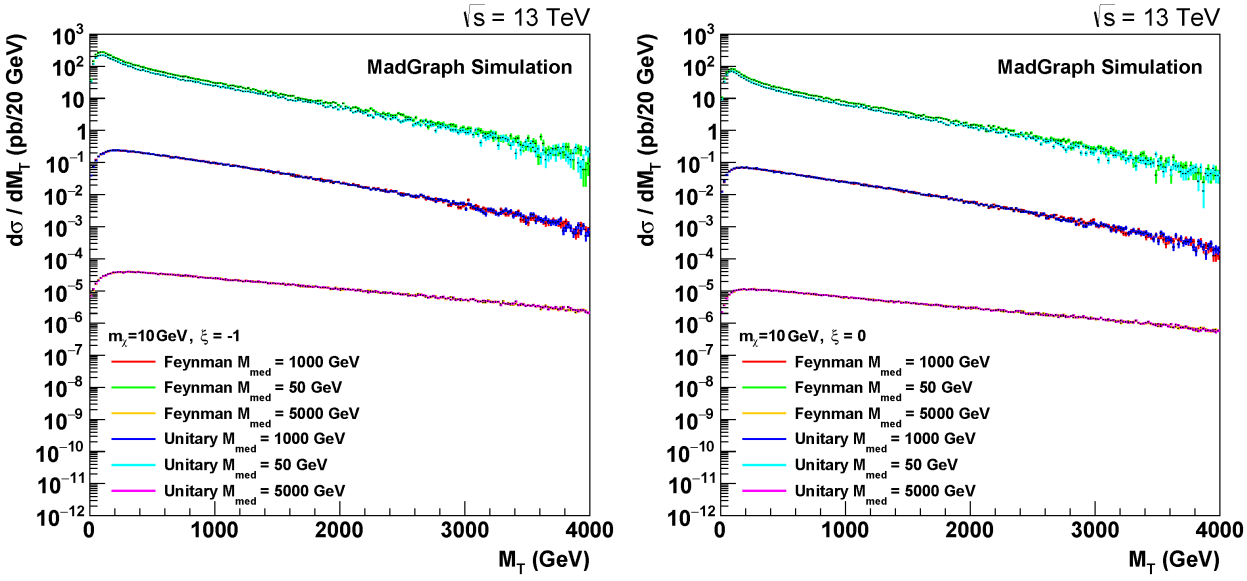

Figure 4.21: Differential cross section for different gauges. Left: $\xi = -1$. Right: $\xi = 0$

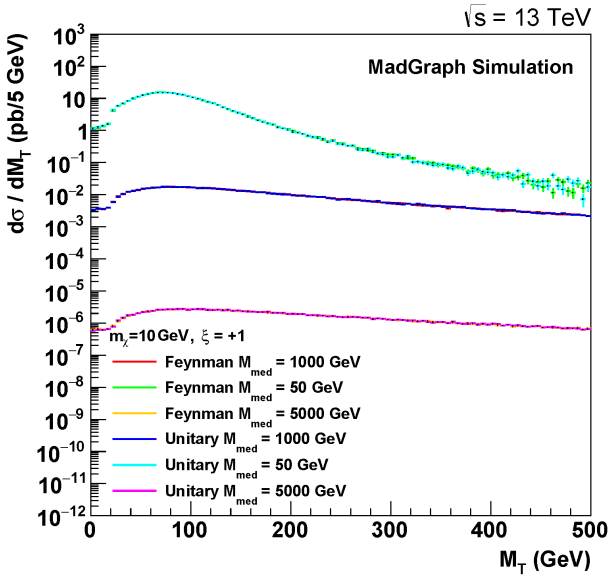

Figure 4.22: Differential cross section for different gauges and $\xi = +1$

Chapter 5

Outlook

5.1 Using Majorana Spinors for the Description of Dark Matter

The most promising and motivating aspect about Majorana dark matter is still the fact, that SUSY's neutralino is a Majorana fermion. This neutralino is often considered as a bright dark matter candidate. If one minds, that SUSY theories are seemingly the only ones that can provide such an explanation for dark matter on particle level, it is much more intuitive to even use Majorana approaches, when working with toy models, like simplified models and EFTs are. Beside being better founded from a theoretical point of view, Majorana dark matter brings along another advantage too. As it was found in this analysis, such an approach supplies a better signal, due to its cross section being a factor of two greater than the cross section of the usual Dirac dark matter approach. Especially when it comes to the validity of ξ, this could be a very good alternative, too. If one considers the cases of $\xi = -1, 0$ still as forbidden, Majorana dark matter's greater cross section could maybe already be enough of an increase for the signal not to disappear in the background.

5.2 Validity of the Cases $\xi = -1, 0$

In the beginning of the section for this parameters validity it was already stated, that one can make a more general discussion about the violation of gauge invariance and unitarity for toy models. Even after seeing this results, this is still an argument that can and will surely be advanced.
Regarding this analysis, it was seen, that there are some important differences between an EFT and a simplified model, that disable a simple application of results for an EFT on the latter one. Although the analysis of the mono-lepton channel's W boson's polarization did not give access to the problem that was investigated, it revealed some differences between those two models. Summarized, these were differences one would necessarily expect, since there is a different intermediate state in the simplified model.
The results of the parton level cross sections analysis and the latter check for gauge invariance provided a strong indication for the validity of $\xi = -1, 0$ within a certain range. Especially the check of the gauge invariance is very important here, since this is the main argument of the paper, which restricts the mentioned cases for an EFT.
But nevertheless, the following point should not be neglected. To properly declare these cases as valid, it is inevitable to make a proper theoretical derivation of the respective Ward identity and check if it is satisfied and if the theory is therefore gauge invariant. Even if this analysis provides an empirical evidence for the mentioned invariance to be existing for

a certain range, this alone is not enough to accept the validity completely without doubt. Hence it was decided not to perform a further analysis on the concrete range of the mentioned cases' validity but stay at the approximate range of 400 GeV $\leq M_{med} \leq$ 15000 GeV. This nevertheless is already a useful range of validity. For a theorist these results should be enough motivation to check the upper mentioned issue.
From a experimental physicists view this should nonetheless be enough evidence to use the cases $\xi = -1, 0$, since these results are a much better basement then just assuming, that the restriction for an EFT can simply be applied to a simplified model as well - at least until a theorist attends to this matter and does the necessary clarification.

Chapter 6

Acknowledgements

In the first place I would like to thank my family and friends for their support in every concern. Especially my beloved parents, who made it possible for me to study physics, deserve my most honest thanks.
Furthermore I would like to thank my mentors Klaas Padeken and Viktor Kutzner for their help in any account and for even using their free time to help me and give advises. This sure is nothing self-evident. I also appreciate the harmonic atmosphere we had in our office, as well as our conversations on rather unphysical topics like history or philosophy. Additionally I want to mention Marcel Materok, who helped me with many technical issues, although he himself is also about to write his bachelor thesis.
I would also like to thank Prof. Dr. Thomas Hebbeker and Dr.Kerstin Höpfner for making it possible for me to write this thesis.

Chapter 7

Appendix

7.1 Theory

7.1.1 Charge Conjugation

The theory of Majorana spinors belongs to *relativistic quantum theory*. The fundamental equations of this theory are the so called Klein-Gordon-Schrödinger[1] equation and the Dirac equation. The Klein-Gordon-Schrödinger equation describes spin 1 particles (bosons), whereas the latter one describes particles with a spin of $\frac{1}{2}$ (fermions). For Majorana spinors the latter one is more relevant.
A Majorana spinor shall describe a fermion that is defined to be a self conjugated particle, whereas conjugated concerns a charge conjugation. Thus such a particle can not have an electrical charge.
The first attempts on the operation of a charge conjugation is due to Paul Dirac's prediction of the existence of a positron. Since the positron was claimed to have the same spin and mass like the electron but another charge, it was obvious that such a particle should also satisfy a respective Dirac equation in a electromagnetic field. Mathematically this means that one searches for transformations

$$\psi(x) \to \psi^c(x) \tag{7.1.1}$$

so, that if $\psi(x)$ satisfies

$$\left(\gamma^\mu \left(i\partial_\mu + eA_\mu\right) - m\right)\psi(x) = 0 \tag{7.1.2}$$

the transformed spinor ψ^c has to satisfy

$$\left(\gamma^\mu \left(i\partial_\mu - eA_\mu\right) - m\right)\psi^c(x) = 0. \tag{7.1.3}$$

A possibility to change the sign between $i\partial_\mu$ and eA_μ in equation 7.1.2 is to use complex conjugation. One can write it as

$$\left(\gamma^\mu \left(i\partial_\mu + eA_\mu\right) - m\right)\gamma^0\gamma^0\psi(x) = 0, \tag{7.1.4}$$

since $\gamma^0\gamma^0 = \mathbb{1}$. A way to complex conjugate a matrix or vector is to adjoin and then transpose it ($A^{\dagger T} = A^*$). Adjoining the matrix equation leads to

$$\psi^\dagger\gamma^0\gamma^0\left(\gamma^{\mu\dagger}\left(-i\overleftarrow{\partial_\mu} + eA_\mu\right) - m\right) = 0. \tag{7.1.5}$$

[1] The most common name for this equation is just "Klein-Gordon". Schrödinger actually found this equation, which is derived by connecting the relativistic energy momentum relation and his famous Schrödinger equation via the correspondence principle, at about the same time and it was therefore decided to also credit him.

The arrow above the derivative indicates that it operates to the left. For the gamma matrices one can derive the relation $\gamma^0\gamma^{\mu\dagger}\gamma^0 = \gamma^\mu$. When multiplying this equation with γ^0 from the right one can use this and hence gets

$$\begin{aligned} &\psi^\dagger\gamma^0\left(\gamma^\mu\left(-i\overleftarrow{\partial_\mu} + eA_\mu\right) - m\right) = 0 \\ \Leftrightarrow\ &\bar{\psi}\left(\gamma^\mu\left(-i\overleftarrow{\partial_\mu} + eA_\mu\right) - m\right) = 0, \end{aligned} \tag{7.1.6}$$

where it was used that $\bar{\psi} = \psi^\dagger\gamma^0$ is the adjoined spinor. The next step to do is transposing the equation. This leads to

$$\begin{aligned} &\left(\gamma^{\mu T}\left(-i\partial_\mu + eA_\mu\right) - m\right)\bar{\psi}^T = 0 \\ \Leftrightarrow\ &\left(-\gamma^{\mu T}\left(i\partial_\mu - eA_\mu\right) - m\right)\bar{\psi}^T = 0. \end{aligned} \tag{7.1.7}$$

The last step to make the above equation equal equation 7.1.3 is finding a matrix that gives $C\gamma^{\mu T}C^{-1} = -\gamma^\mu$. This can be seen by multiplying the the equation with a matrix C from left and inserting a $C^{-1}C = \mathbb{1}$ between the operators and the spinor:

$$C\left(-\gamma^{\mu T}\left(i\partial_\mu - eA_\mu\right) - m\right)C^{-1}C\bar{\psi}^T = 0. \tag{7.1.8}$$

Such a matrix is in the Dirac basis given by

$$C = i\gamma^2\gamma^0 = i\begin{pmatrix} 0 & -\sigma_2 \\ -\sigma_2 & 0 \end{pmatrix} = \begin{pmatrix} 0 & 0 & 0 & -1 \\ 0 & 0 & 1 & 0 \\ 0 & -1 & 0 & 0 \\ 1 & 0 & 0 & 0 \end{pmatrix}, \tag{7.1.9}$$

with the properties $C^{-1} = C^\dagger = C^T = -C$. Using this matrix one can write

$$\left(\gamma^\mu\left(i\partial_\mu - eA_\mu\right) - m\right)C\bar{\psi}^T = 0 \tag{7.1.10}$$

and find ψ^c to be defined as

$$\psi^c = C\bar{\psi}^T. \tag{7.1.11}$$

7.1.2 Majorana Spinors

For the derivation of a Majorana spinor the Weyl basis will be used, which is often also referred to as the chiral basis. The latter name is due to the fact, that in this basis a spinor can be portrayed by its chiral amounts, like

$$\chi = \begin{pmatrix} \chi_R \\ \chi_L \end{pmatrix}. \tag{7.1.12}$$

Performing a charge conjugation for this spinor gives

$$\begin{aligned} \chi^c &= i\gamma^2\gamma^0\left(\chi^\dagger\gamma^0\right)^T = i\gamma^2\gamma^0\gamma^0\chi^* \\ \begin{pmatrix} \chi_R^c \\ \chi_L^c \end{pmatrix} &= \begin{pmatrix} 0 & i\sigma_2 \\ -i\sigma_2 & 0 \end{pmatrix}\begin{pmatrix} \chi_R^* \\ \chi_L^* \end{pmatrix} = \begin{pmatrix} i\sigma_2\chi_L^* \\ -i\sigma_2\chi_R^* \end{pmatrix} \overset{!}{=} \begin{pmatrix} \chi_R \\ \chi_L \end{pmatrix} \end{aligned} \tag{7.1.13}$$

Possible solutions of this equation are

$$\chi_R^M = \begin{pmatrix} \chi_R \\ -i\sigma_2\chi_R^* \end{pmatrix} \qquad \text{and} \qquad \chi_L^M = \begin{pmatrix} i\sigma_2\chi_L^* \\ \chi_L \end{pmatrix}. \tag{7.1.14}$$

7.2 M_T Spectra

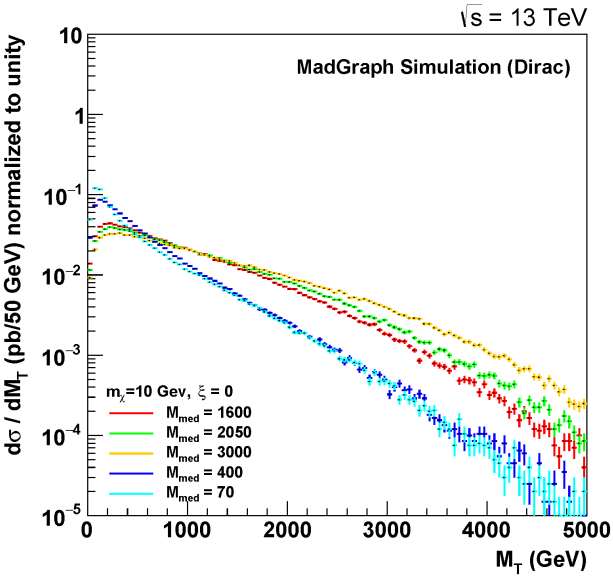

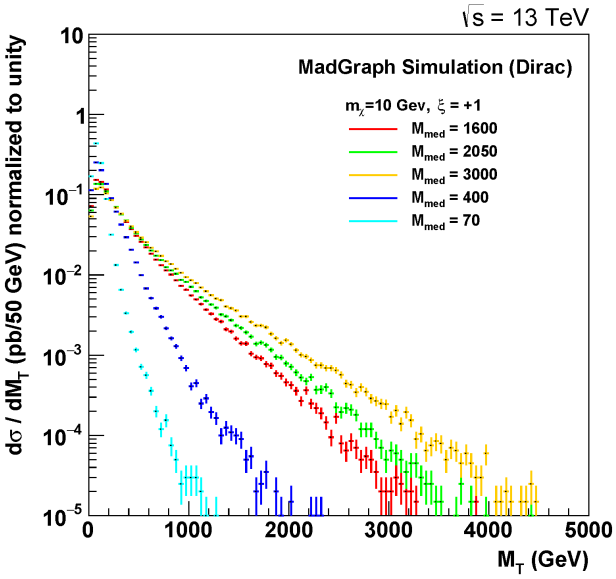

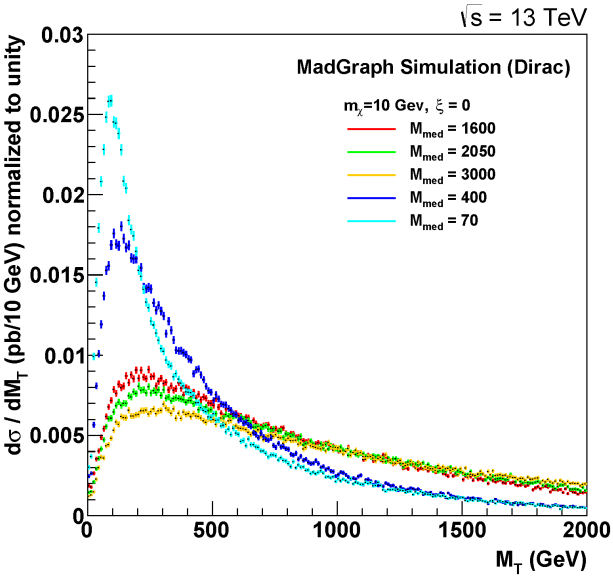

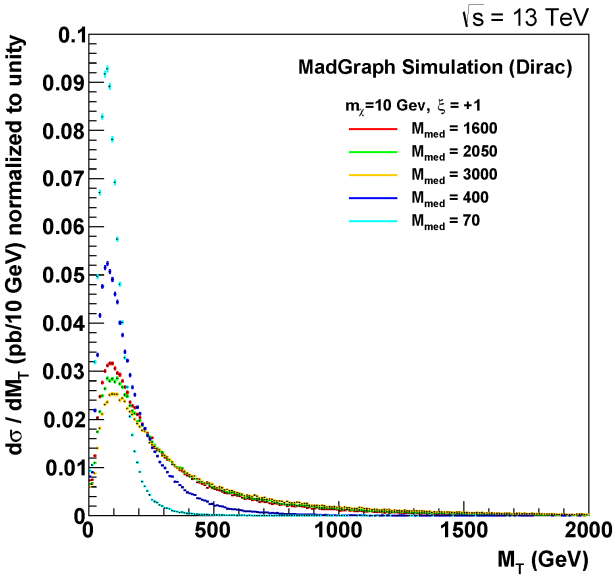

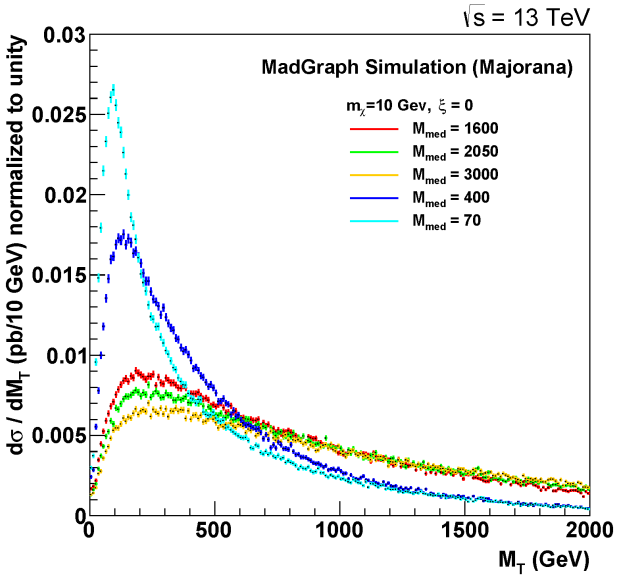
√s = 13 TeV
MadGraph Simulation (Majorana)
m_χ=10 Gev, ξ = 0
M_med = 1600
M_med = 2050
M_med = 3000
M_med = 400
M_med = 70
dσ / dM_T (pb/10 GeV) normalized to unity
M_T (GeV)

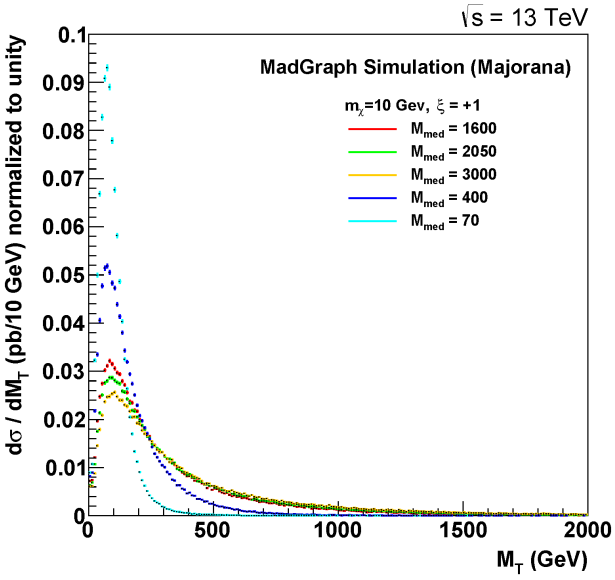
√s = 13 TeV
MadGraph Simulation (Majorana)
m_χ=10 Gev, ξ = +1
M_med = 1600
M_med = 2050
M_med = 3000
M_med = 400
M_med = 70
dσ / dM_T (pb/10 GeV) normalized to unity
M_T (GeV)

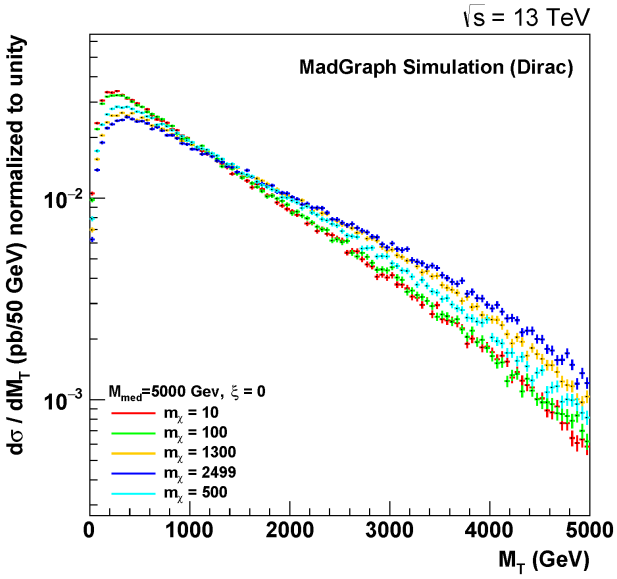
√s = 13 TeV
MadGraph Simulation (Dirac)
M_med=5000 Gev, ξ = 0
m_χ = 10
m_χ = 100
m_χ = 1300
m_χ = 2499
m_χ = 500
dσ / dM_T (pb/50 GeV) normalized to unity
M_T (GeV)

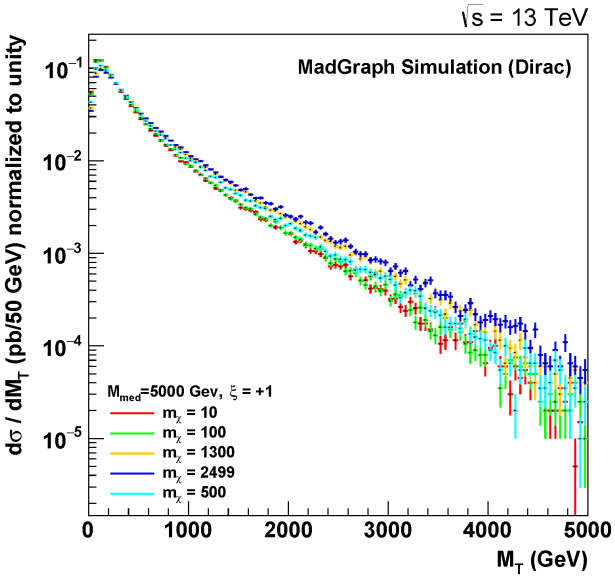
√s = 13 TeV
MadGraph Simulation (Dirac)
M_med=5000 Gev, ξ = +1
m_χ = 10
m_χ = 100
m_χ = 1300
m_χ = 2499
m_χ = 500
dσ / dM_T (pb/50 GeV) normalized to unity
M_T (GeV)

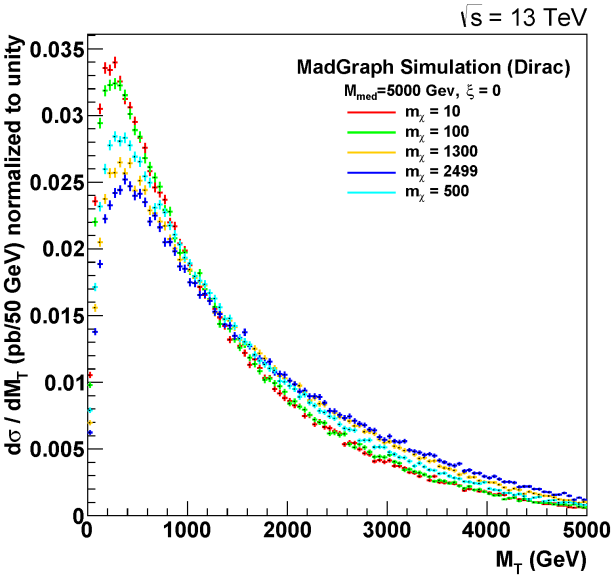
√s = 13 TeV
MadGraph Simulation (Dirac)
M_med=5000 Gev, ξ = 0
m_χ = 10
m_χ = 100
m_χ = 1300
m_χ = 2499
m_χ = 500
dσ / dM_T (pb/50 GeV) normalized to unity
M_T (GeV)

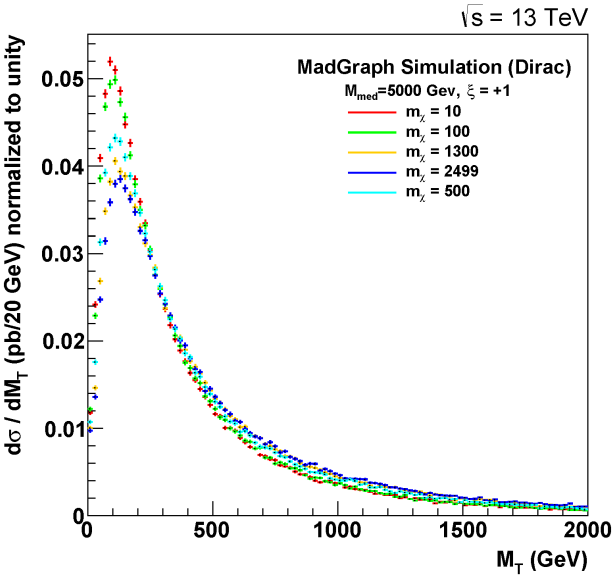
√s = 13 TeV
MadGraph Simulation (Dirac)
M_med=5000 Gev, ξ = +1
m_χ = 10
m_χ = 100
m_χ = 1300
m_χ = 2499
m_χ = 500
dσ / dM_T (pb/20 GeV) normalized to unity
M_T (GeV)

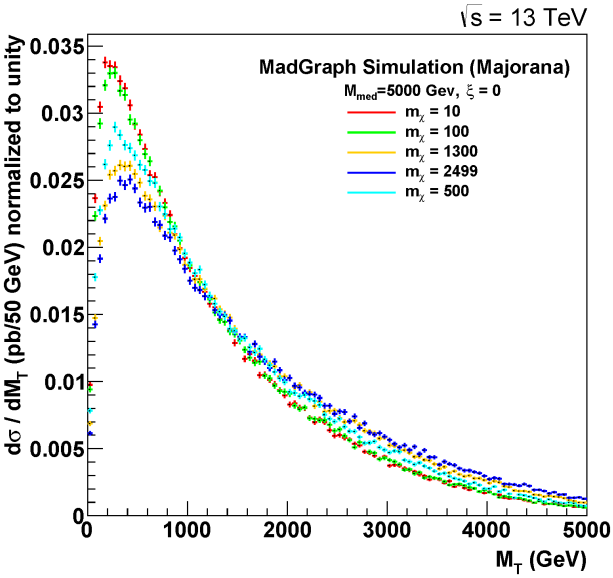
√s = 13 TeV
MadGraph Simulation (Majorana)
M_med=5000 Gev, ξ = 0
m_χ = 10
m_χ = 100
m_χ = 1300
m_χ = 2499
m_χ = 500
dσ / dM_T (pb/50 GeV) normalized to unity
M_T (GeV)

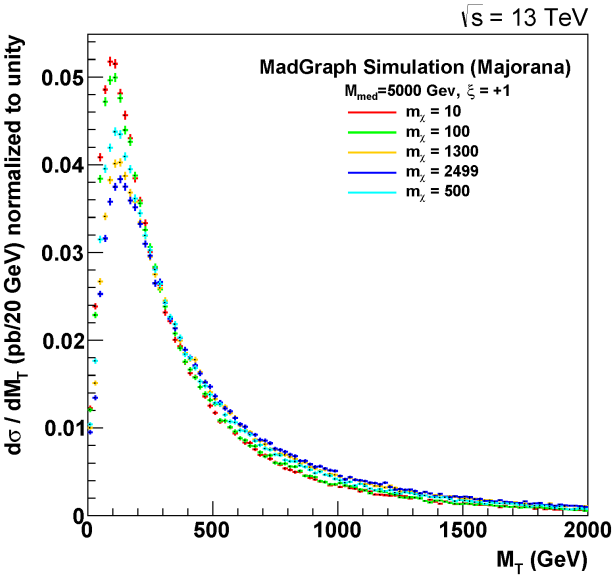
√s = 13 TeV
MadGraph Simulation (Majorana)
M_med=5000 Gev, ξ = +1
m_χ = 10
m_χ = 100
m_χ = 1300
m_χ = 2499
m_χ = 500
dσ / dM_T (pb/20 GeV) normalized to unity
M_T (GeV)

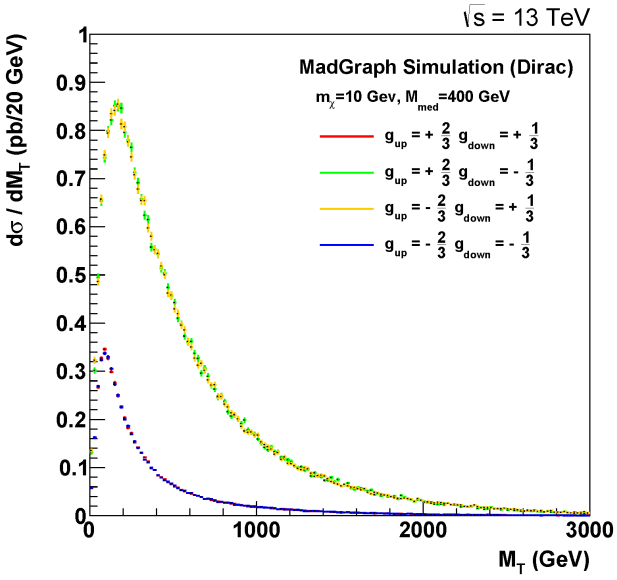
√s = 13 TeV
MadGraph Simulation (Dirac)
m_χ=10 Gev, M_med=400 GeV
g_up = + 2/3 g_down = + 1/3
g_up = + 2/3 g_down = - 1/3
g_up = - 2/3 g_down = + 1/3
g_up = - 2/3 g_down = - 1/3
dσ / dM_T (pb/20 GeV)
M_T (GeV)

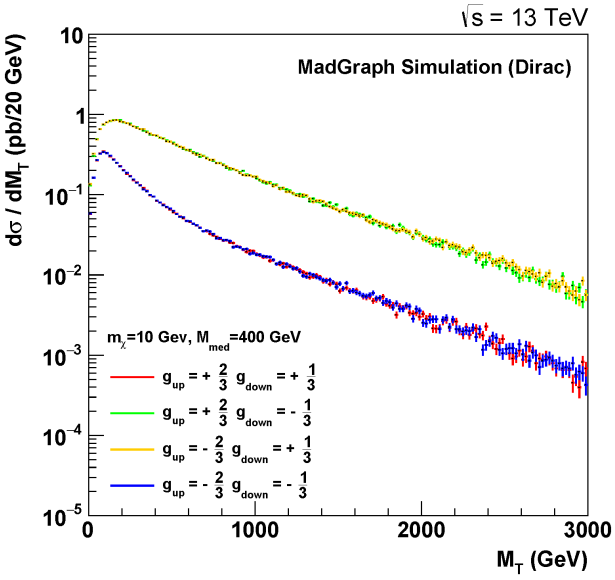
√s = 13 TeV
MadGraph Simulation (Dirac)
m_χ=10 Gev, M_med=400 GeV
g_up = + 2/3 g_down = + 1/3
g_up = + 2/3 g_down = - 1/3
g_up = - 2/3 g_down = + 1/3
g_up = - 2/3 g_down = - 1/3
dσ / dM_T (pb/20 GeV)
M_T (GeV)

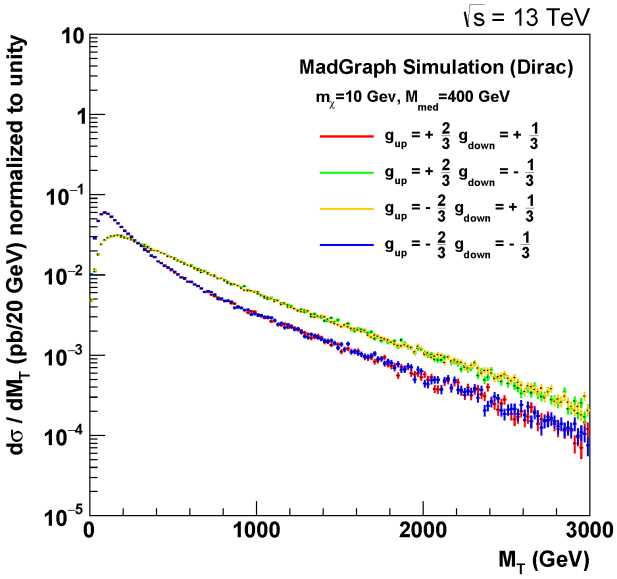
√s = 13 TeV
MadGraph Simulation (Dirac)
m_χ=10 Gev, M_med=400 GeV
g_up = + 2/3 g_down = + 1/3
g_up = + 2/3 g_down = - 1/3
g_up = - 2/3 g_down = + 1/3
g_up = - 2/3 g_down = - 1/3
dσ / dM_T (pb/20 GeV) normalized to unity
M_T (GeV)

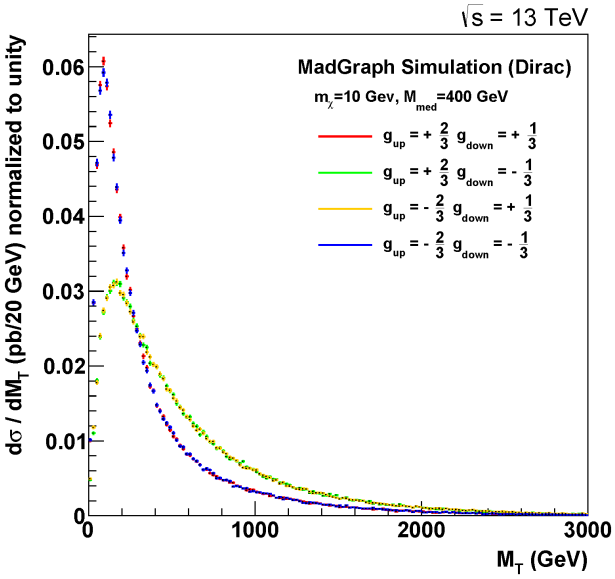
√s = 13 TeV
MadGraph Simulation (Dirac)
m_χ=10 Gev, M_med=400 GeV
g_up = + 2/3 g_down = + 1/3
g_up = + 2/3 g_down = - 1/3
g_up = - 2/3 g_down = + 1/3
g_up = - 2/3 g_down = - 1/3
dσ / dM_T (pb/20 GeV) normalized to unity
M_T (GeV)

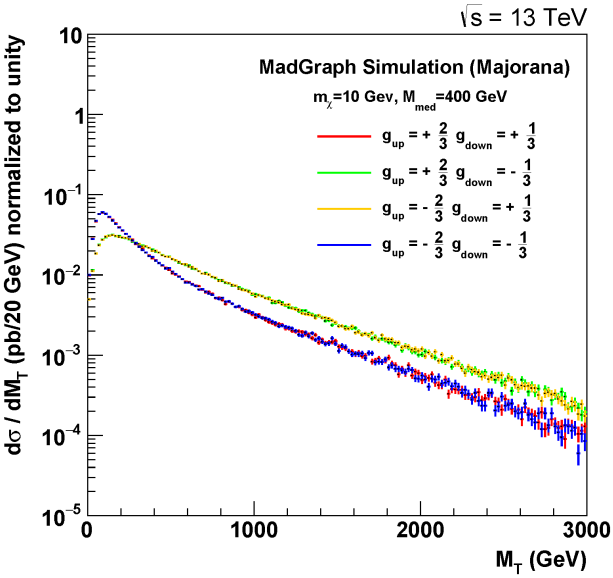
√s = 13 TeV
MadGraph Simulation (Majorana)
m_χ=10 Gev, M_med=400 GeV
g_up = + 2/3 g_down = + 1/3
g_up = + 2/3 g_down = - 1/3
g_up = - 2/3 g_down = + 1/3
g_up = - 2/3 g_down = - 1/3
dσ / dM_T (pb/20 GeV) normalized to unity
M_T (GeV)

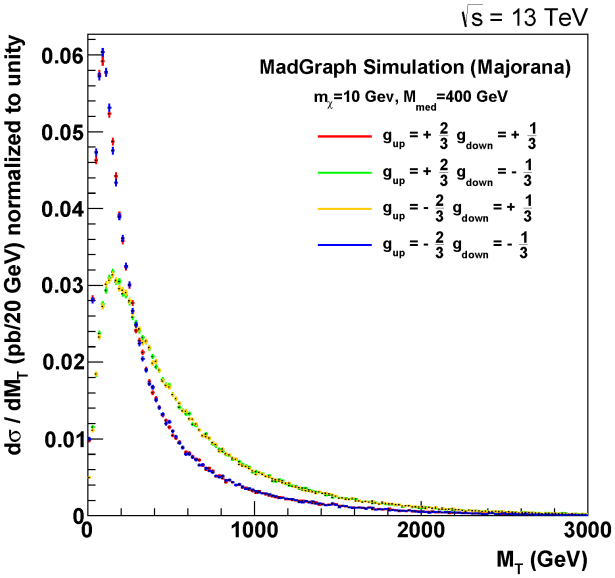
√s = 13 TeV
MadGraph Simulation (Majorana)
m_χ=10 Gev, M_med=400 GeV
g_up = + 2/3 g_down = + 1/3
g_up = + 2/3 g_down = - 1/3
g_up = - 2/3 g_down = + 1/3
g_up = - 2/3 g_down = - 1/3
dσ / dM_T (pb/20 GeV) normalized to unity
M_T (GeV)

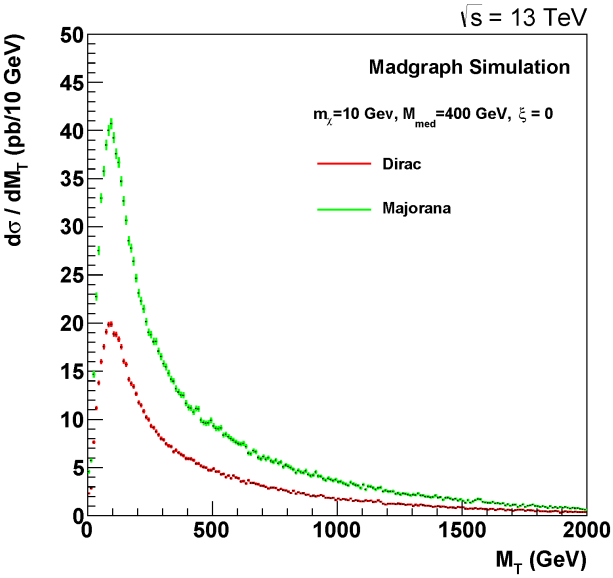
√s = 13 TeV
Madgraph Simulation
m_χ=10 Gev, M_med=400 GeV, ξ = 0
Dirac
Majorana
dσ / dM_T (pb/10 GeV)
M_T (GeV)

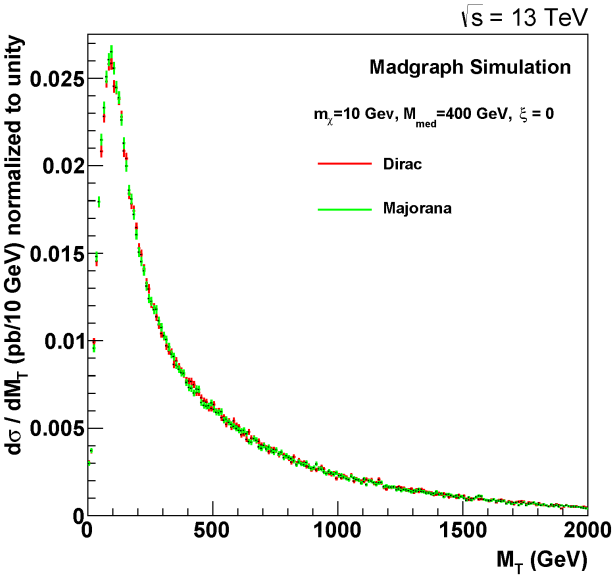
√s = 13 TeV
Madgraph Simulation
m_χ=10 Gev, M_med=400 GeV, ξ = 0
Dirac
Majorana
dσ / dM_T (pb/10 GeV) normalized to unity
M_T (GeV)

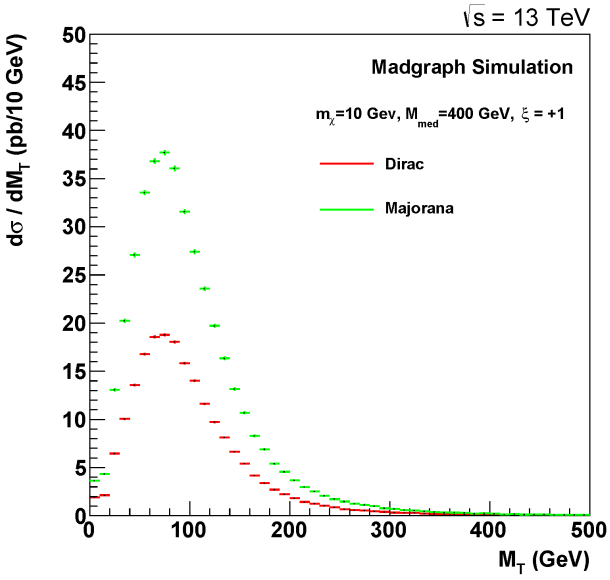
√s = 13 TeV
Madgraph Simulation
m_χ=10 Gev, M_med=400 GeV, ξ = +1
Dirac
Majorana
dσ / dM_T (pb/10 GeV)
M_T (GeV)

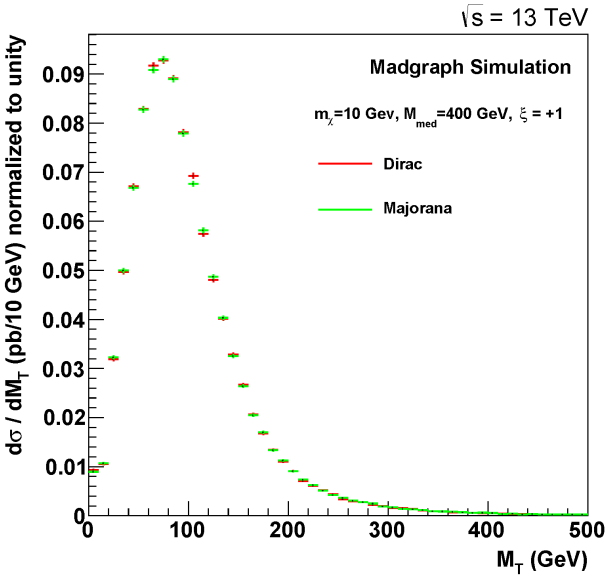
√s = 13 TeV
Madgraph Simulation
m_χ=10 Gev, M_med=400 GeV, ξ = +1
Dirac
Majorana
dσ / dM_T (pb/10 GeV) normalized to unity
M_T (GeV)

7.3 Polarization Plots

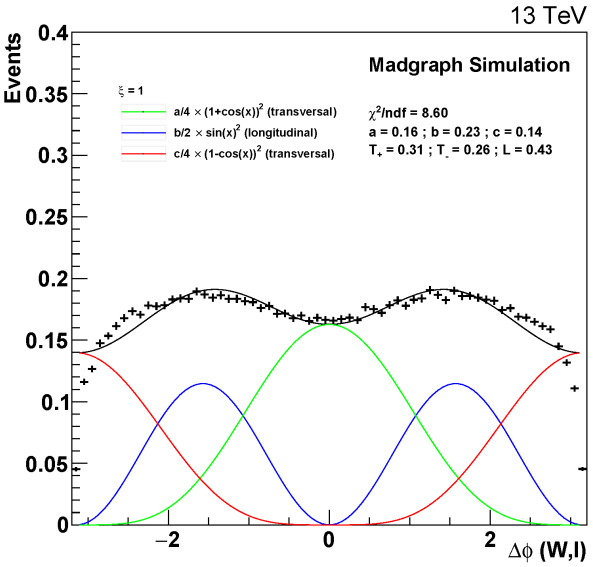

(a) Pol(u) = +100, Pol(d) = +100

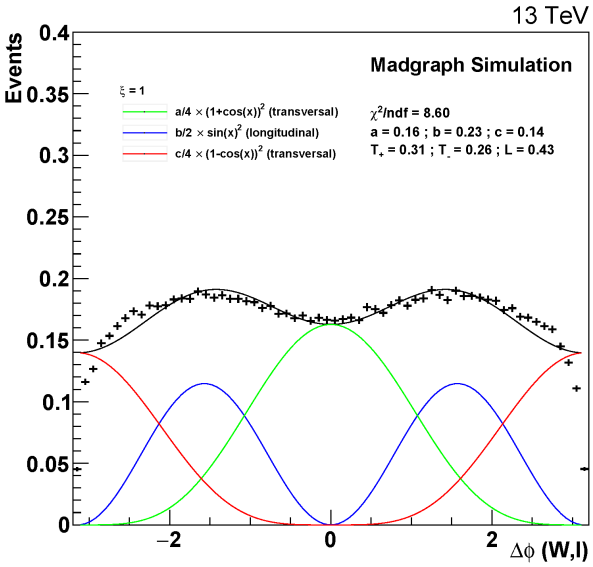

(b) Pol(u) = +100, Pol(d) = -100

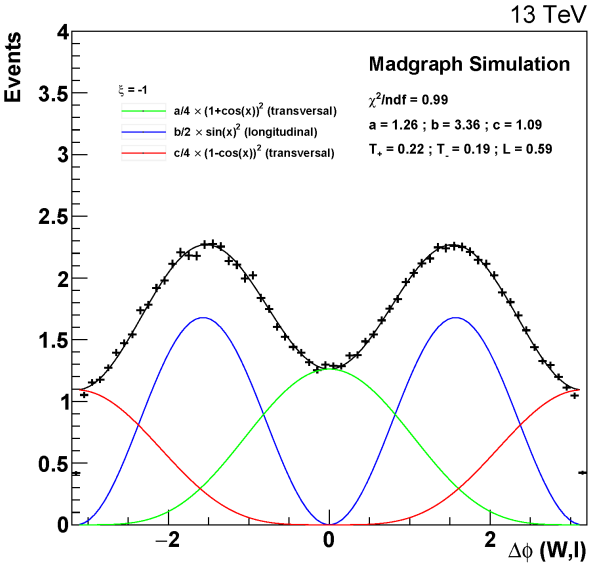

(a) Pol(u) = +100, Pol(d) = +100

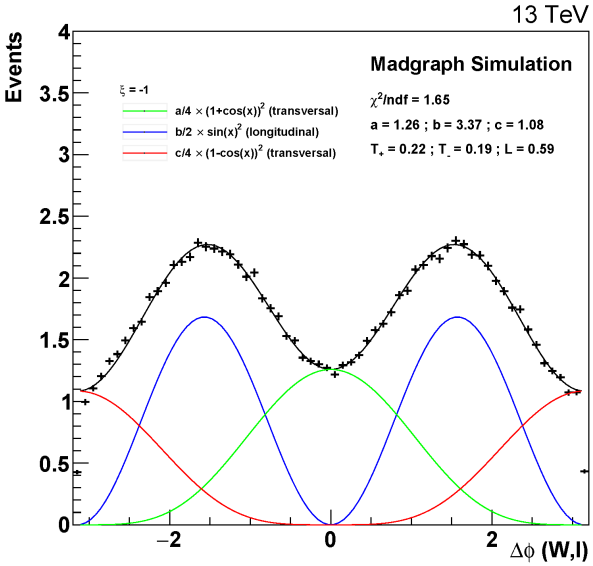

(b) Pol(u) = +100, Pol(d) = -100

7.4 Parton Level Cross Section

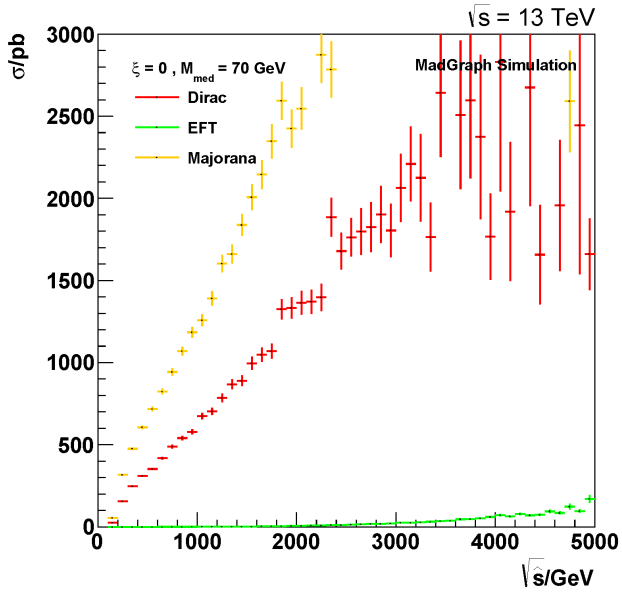

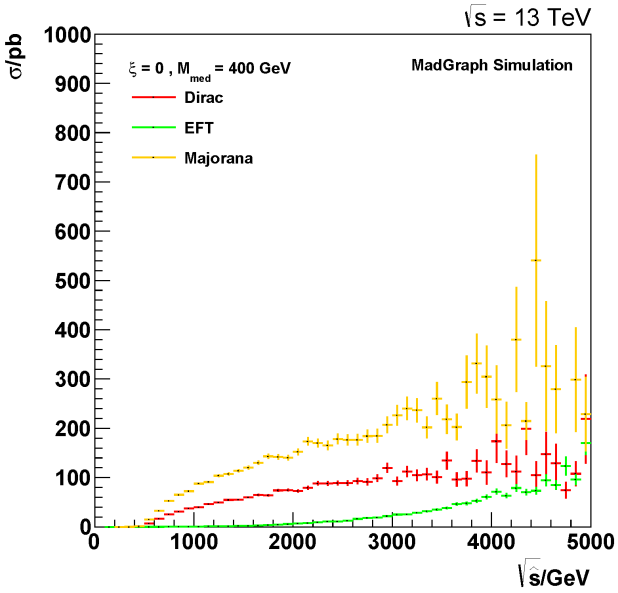

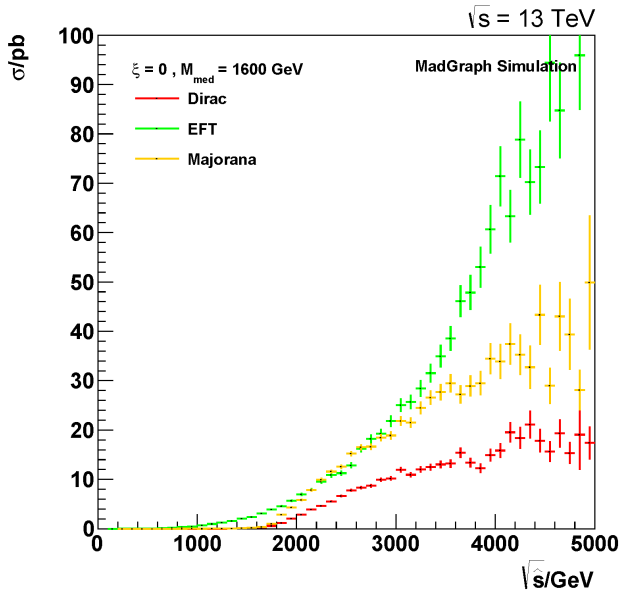

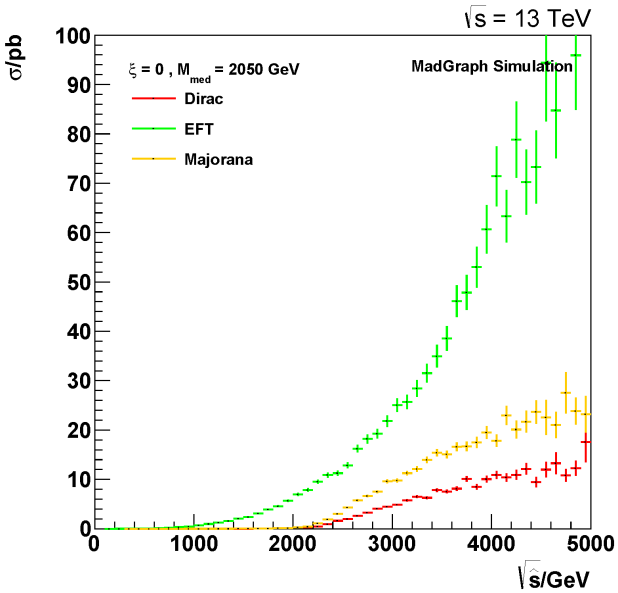

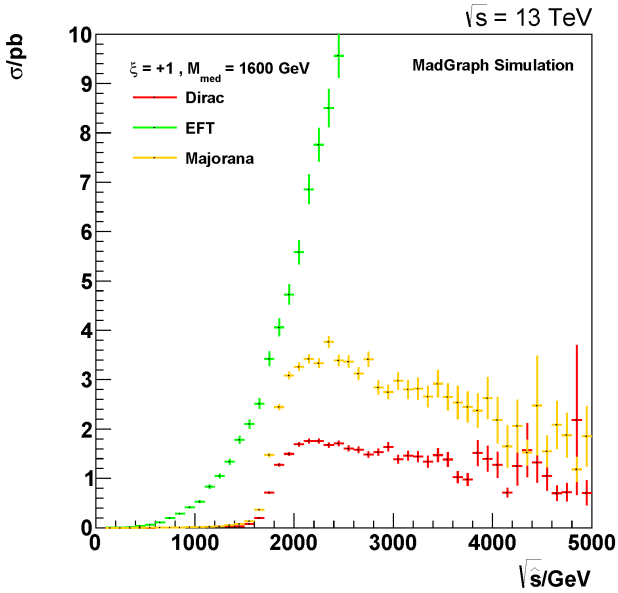
√s = 13 TeV
ξ = +1 , M_med = 1600 GeV
MadGraph Simulation
Dirac
EFT
Majorana
σ/pb
√ŝ/GeV

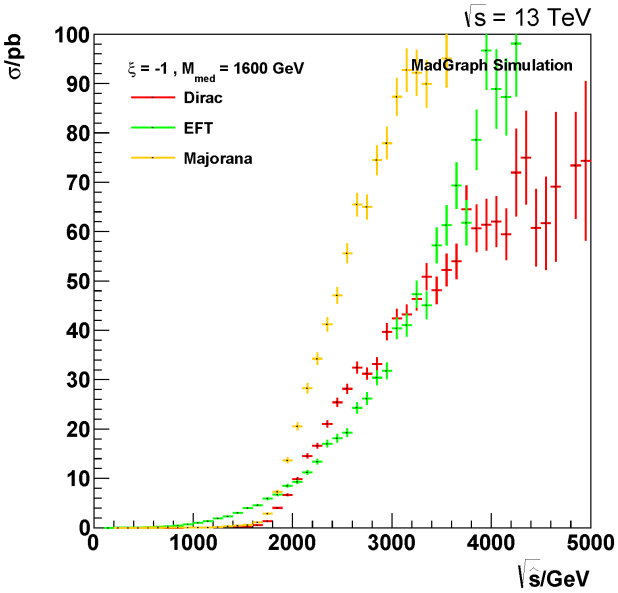
√s = 13 TeV
ξ = -1 , M_med = 1600 GeV
MadGraph Simulation
Dirac
EFT
Majorana
σ/pb
√ŝ/GeV

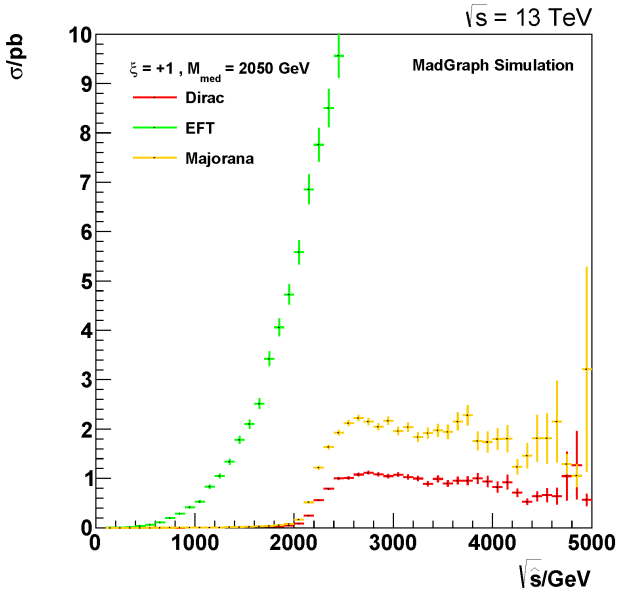
√s = 13 TeV
ξ = +1 , M_med = 2050 GeV
MadGraph Simulation
Dirac
EFT
Majorana
σ/pb
√ŝ/GeV

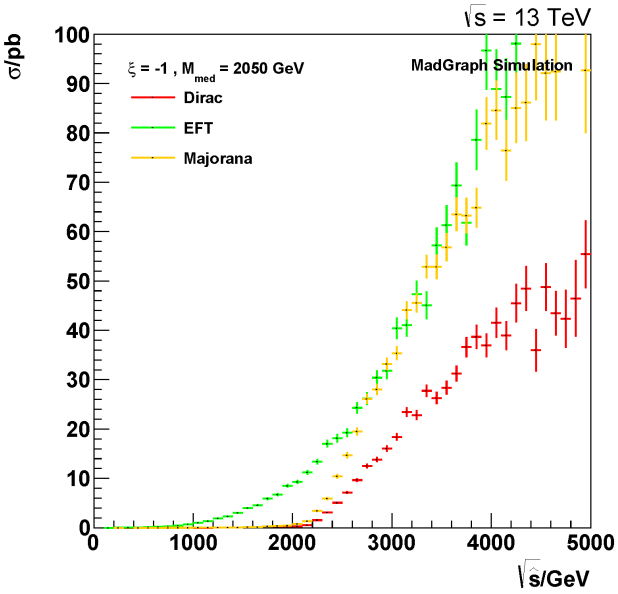
√s = 13 TeV
ξ = -1 , M_med = 2050 GeV
MadGraph Simulation
Dirac
EFT
Majorana
σ/pb
√ŝ/GeV

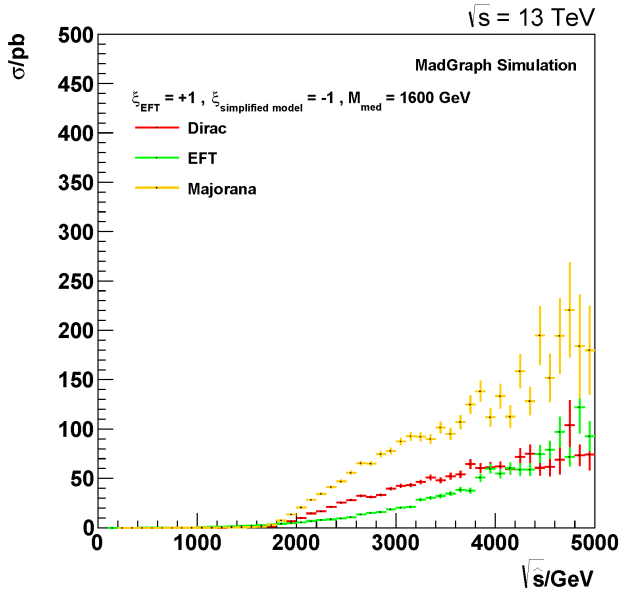
√s = 13 TeV
MadGraph Simulation
ξ_EFT = +1 , ξ_simplified model = -1 , M_med = 1600 GeV
Dirac
EFT
Majorana
σ/pb
√ŝ/GeV

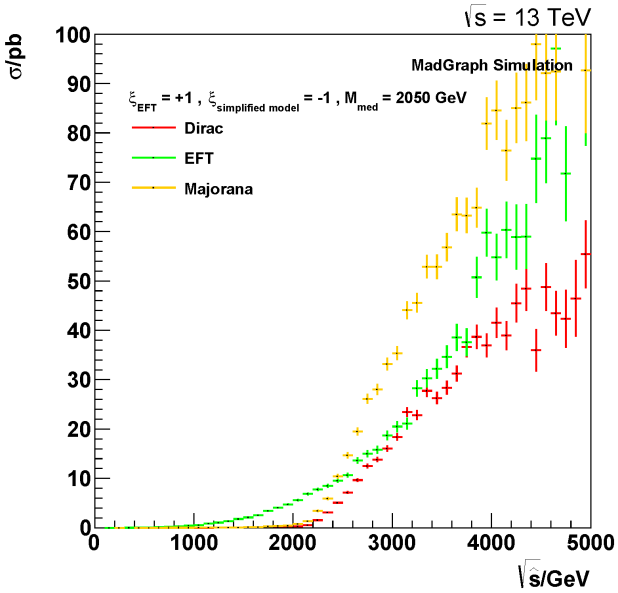
√s = 13 TeV
MadGraph Simulation
ξ_EFT = +1 , ξ_simplified model = -1 , M_med = 2050 GeV
Dirac
EFT
Majorana
σ/pb
√ŝ/GeV

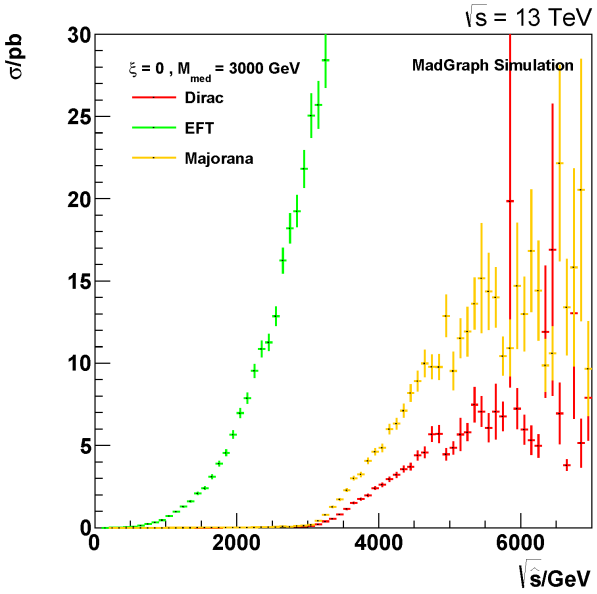
√s = 13 TeV
MadGraph Simulation
ξ = 0 , M_med = 3000 GeV
Dirac
EFT
Majorana
σ/pb
√ŝ/GeV

7.5 Conventions

In this analysis natural units are used, where $\hbar = c = 1$. For sums Einstein's sum convention is used with

$$x^\mu x_\mu = \sum_\mu x^\mu x_\mu = \sum_{\mu\nu} x_\mu x_\nu g^{\mu\nu},$$

with the metric tensor $g^{\mu\nu}$ being defined as

$$g^{\mu\nu} = \begin{pmatrix} 1 & 0 & 0 & 0 \\ 0 & -1 & 0 & 0 \\ 0 & 0 & -1 & 0 \\ 0 & 0 & 0 & -1 \end{pmatrix}$$

and $g^{\mu\nu} = g_{\mu\nu}$.
The greek symbol ψ is used for arbitrary solutions of the Dirac equation and χ for the spinors of DM. Arbitrary axial vector quantities are labeled as A^μ.

Bibliography

[1] Jalal Abdallah et al., *Simplified Models for Dark Matter and Missing Energy Searches at the LHC*, October 2014, arXiv:1409.2893.

[2] Michael Duerr, Pavel Fileviez Perez and Juri Smirnov, *Simplified Dirac Dark Matter Models*, June 2015, arXiv:1506.05107.

[3] Daniele Alves et al. (LHC New Physics Working Group), *Simplified Models for LHC New Physics Searches*, May 2011, arXiv:1105.2838.

[4] Jalal Abdallah et al., *Simplified Models for Dark Matter Searches at the LHC* , June 2015, arXiv:1506.0311.

[5] Oliver Buchmueller, Matthew J. Dolan, Sarah A. Malik and Christopher McCabe, *Characterising dark matter searches at colliders and direct detection experiments: Vector mediators*, January 2015, arXiv:1407.8257.

[6] O. Buchmueller, Matthew J. Dolan and Christopher McCabe, *Beyond effective field theory for dark matter searches at the LHC*, August 2013, arXiv:1308.6799.

[7] Nicole F. Bell, Yi Cai, James B. Dent, Rebecca K. Leane and Thomas J. Weiler, *Dark matter at the LHC: EFTs and gauge invariance*, March 2015, arXiv:1503.07874.

[8] Yang Bai and Tim M.P. Tait, *Searches with Mono-Leptons*, June 2013, arXiv:1208.4361.

[9] Beshtoev Kh. M., *Is neutrino produced in standard weak interactions a Dirac or a Majorana particle?*, December 2009, arXiv:0912.0210.

[10] Boris Kayser and Robert E. Shrock, *Distinguishing between Dirac and Majorana neutrinos in neutral-current reactions*, October 1981, Physics Letters, Volume 112B number 2.

[11] M.Zralek, *On the possibilities of distinguishing Dirac from Majorana neutrinos*, November 1997, Acta Physica Polonica B, Vol.28 No. 11.

[12] Prateek Agrawal, Zackaria Chacko, Can Kilic and Rashmish K. Mishra, *A classification of Dark Matter Candidates with Primarily Spin-Dependent Interactions with Matter*, June 2010, arXiv:1003.1912.

[13] Yang Bai and Joshua Berger, *Fermion Portal Dark Matter*, June 2014, arXiv:1308.0612.

[14] CMS PAS EXO-13-004, *Search for dark matter in the mono-lepton channel with pp collision events at* $\sqrt{s}$*=8TeV*, July 2013.

[15] CMS-EXO-12-060, *Search for physics beyong the standard model in final states with a leptin and missing transverse energy in proton-proton collisions at* $\sqrt{s}$*=8TeV*, June 2015, arXiv:1408.2745.

[16] Prof.Dr. Werner Bernreuther, *Relativistische Quantentheorie* (lecture notes), July 2014.

[17] Gianfranco Bertone et al., *Particle Dark Matter: Observations, Models and Searches*, Cambridge University Press, 2010.

[18] Prof. Dr. Eckhard Rebhan, *Quantenfeldtheorie*, Springer-Verlag Berlin, Heidelberg 2010.

[19] Particle Data Group, *Particle Physics Booklet*, July 2014.

[20] Particle Data Group, *Review of Particle Physics*, 2014.

[21] `http://cms.cern.ch/iCMS/analysisadmin/cadilines?id=1312&ancode=EXO-14-007&tp=an&line=EXO-14-007`

[22] Jonathan L. Rosner, *The Standard Model in 2001*, August 2001, arXiv:hep-ph/0108195.

[23] A. Pich, *The Standard Model of Electroweak Interactions*, February 2005, arXiv:hep-ph/0502010.

[24] CMS Collaboration, *The CMS experiment at the CERN LHC*, August 2008.

[25] Tao Han, Zhen Liu and Shufang Su, *Light Neutralino Dark Matter: Direct/Indirect Detection and Collider Searches*, June 2014, arXiv:1406.1181.

[26] Dennis Nick Noll, *A Study of Dark Matter Models at $\sqrt{s}$ = 13 TeV pp Collisions for Mono Lepton Searches*, Bachelor Thesis, September 2015.

[27] C. F. Uhlemann and N. Kauer, *Narrow-width approximation accuracy*, July 2008, arXiv:0807.4112.

[28] J. C. Helo, M. Hirsch, T. Ota and F. A. Pereira dos Santos, *Double beta decay and neutrino mass models*, February 2015, arXiv:1502.05188.

[29] `http://www.hep.phy.cam.ac.uk/~thomson/lectures/partIIIparticles/Handout13_2009.pdf`

[30] `http://www.quantumdiaries.org/wp-content/uploads/2014/10/detection1.png`

[31] `https://cms-docdb.cern.ch/cgi-bin/PublicDocDB/RetrieveFile?docid=11514&version=1&filename=cms_120918_03.png`

[32] `http://i.stack.imgur.com/xgVsI.png`

[33] `http://bustard.phys.nd.edu/Phys171/lectures/dm.html`

[34] `http://www.physik.uzh.ch/groups/serra/images/SM1.png`

Selbstständigkeitserklärung:
Hiermit erkläre ich, dass ich die vorliegende Arbeit eigenständig verfasst habe. Desweiteren habe ich Zitate kenntlich gemacht und keine anderen als die angegebenen Hilfsmittel und Quellen verwendet.

Aachen, den 01.10.2015 Harun Acaroğlu